2017

# Process Parameter Optimization with Numerical modelling and Experimentation design of Binder Jet Additive Manufacturing

Sairam Vangapally
*Minnesota State University, Mankato*

# PROCESS PARAMETER OPTIMIZATION WITH NUMERICAL MODELLING AND EXPERIMENTATION DESIGN OF BINDER JET ADDITIVE MANUFACTURING

A Thesis Submitted in Partial Fulfillment of the Requirements

for the Degree of Master of Science in

Mechanical Engineering

By

Sairam Vangapally

**MINNESOTA STATE UNIVERSITY, MANKATO**

October 2017

The thesis of Sairam Vangapally is approved on 10/13/2017:

| | |
|---|---|
| Dr. Shaobiao Cai, PE-Assistant Professor | Date |
| Dr. Jin Y. Park, Professor | Date |
| Dr. Kuldeep Agarwal, Assistant Professor | Date |

Minnesota State University, Mankato

# ABSTRACT

Binder jetting technology is an additive manufacturing technology in which powder materials are binded together layer by layer forming the product from input CAD model. The process involves printing the product layer by layer, curing and sintering. The mechanical properties of 3D printed samples varies based on process parameters, hence there is a need to tune the process parameters for optimal characteristics. Three main parameters namely layer thickness, sintering time and sintering temperature were identified and the study focuses on the effect of parameters on dimensional accuracy and compressive strength of the samples. Full factorial experimental approach was used to conduct the experiments and analysis of variance was performed to determine the significance of parameters. Along with parameters optimization, feed forward back propagation artificial neural network model is developed to quantify the relationship between three parameters and compressive strength, the model is developed based on experimental data and validated with known data.

Also, Compressive behavior of four lattice designs considered in the study were simulated by finite element analysis and numerical results were compared with experimental data in order to validate the finite element model. FE models of different lattice designs were developed from experimental test data using ANSYS and the simulated compressive behavior is compared to that experimental compression test results.

Dedicated to my parents, advisor and friends, I couldn't have done this without you. Thank you for all your support along the way.

# ACKNOWLEDGMENTS

Firstly, I would like to thank my advisor, Dr. Shaobiao Cai for providing me the opportunity to work on this project. I am grateful to him for his patience and guidance throughout the thesis work. I would like to express my sincere gratitude to Dr. Jin Y Park for his suggestions and support during my graduate study. Special thanks to Dr. Kuldeep Agarwal for his suggestions and guidance during the experimentation work. I would like to thank all the three committee members for their continuous support and encouragement throughout my graduate study. I would like to thank Mr. Kevin Schull for providing a great environment for accompanying research in the laboratory. Lastly, I would like to thank my parents and friends for their continued support for helping me to achieve my objectives.

TABLE OF CONTENTS

**CHAPTER 1** ..... **1**

**1.0 Introduction** ..... **1**

**1.1 Research Objectives and Scope** ..... **11**

**CHAPTER 2** ..... **13**

**2.0 Process and Approaches** ..... **13**

**2.1 Experimental Method and Design** ..... **13**

**2.1.1 Full Factorial Design of Experiments** ..... **15**

**2.1.2 Sample Preparation** ..... **17**

**2.1.3 Compression Testing** ..... **17**

**2.1.4 Main and Interaction Effect plots** ..... **18**

**2.1.5 Analysis of Variance** ..... **18**

**2.2 Neural Network Model** ..... **21**

**2.3 Finite Element Modelling** ..... **26**

**2.3.1 Designs** ..... **26**

**2.3.2 Material Properties** ..... **27**

**CHAPTER 3** ..... **29**

**3.0 Results and Discussion** ..... **29**

**3.1 Experimental Analysis: Effect of Build Parameters** ..... **29**

**3.1.1 Solid Structure** ..... **30**

**3.1.2 Circular Lattice Structure** ..... **38**

**3.1.3 Cubical Lattice Structure** ..... **41**

**3.1.4 Discussion** ..... **44**

**3.2 Neural Network Results** ..... **47**

**3.2.1 Solid Structure ..... 47**
**3.2.2 Circular Lattice Structure ..... 50**
**3.2.3 Cubical Lattice Structure ..... 52**
**3.2.4 Model Validation ..... 56**

**3.3 Finite Element Analysis ..... 58**
**3.3.1 Finite element simulation of solid ..... 59**
**3.3.2 Finite element simulation of four lattice structures ..... 60**

**3.4 Applications ..... 64**

**3.5 Conclusion and Suggestion for Future work ..... 66**

**4 BIBLIOGRAPHY ..... 68**

**LIST OF FIGURES**

Figure 1.0-1: Schematic representation of binder jetting process [21] ..... 4

Figure 1.0-2: Fishbone diagram representing various parameters involved in the process ..... 5

Figure 1.0-3: Neural Network Schematic representation ..... 8

Figure 2.1-1: Flow Diagram of Experimental Methodology ..... 13

Figure 2.1-2: (a) ExOne M-lab machine, (b) Radial shrinkage and longitudinal shrinkage directions ..... 15

Figure 2.1-3: Binder jet additive manufactured solid cylindrical sample ..... 17

Figure 2.1-4: Sample in between compression platens of MTS Machine ..... 18

Figure 2.2-1: Neural Network Schematic representation, Where A-Layer thickness, B-Sintering time, C-Sintering temperature, O-Compressive Strength, Σ represents summation & F(x) is activation function, b1 & b2 are bias ..... 22

Figure 2.2-2: Flow chart showing the entire training process and the parameters involved. ..... 25

Figure 2.3-1: Finite element Analysis Methodology ..... 26

Figure 2.3-2:(a) Cubical unit cell (b) Circular unit cell (c) Circular 1 (d) Cubical 1 (e) Circular 2 (f) Cubical 2 ..... 27

Figure 2.3-3: Binder jetting fabricated samples of various lattice structures ..... 28

Figure 3.1-1: Main effects plot of process parameters on compressive strength, A-Layer thickness (low- 50 µm, high- 100 µm), B-Sintering time (low- 2hours, high- 4 hours), C-Sintering temperature (low- 1120 $^{o}$C, high- 1180$^{o}$C) ..... 31

Figure 3.1-2: Interaction effects plot of process parameters on compressive strength, A*B refers interaction between Layer thickness and Sintering time, A*C refers interaction

between Layer thickness and Sintering temperature, B*C refers interaction between Sintering temperature and Sintering time ..... 32

Figure 3.1-3: Main effects plot of process parameters on radial shrinkage rate, A-Layer thickness (low- 50 µm, high- 100 µm), B-Sintering time (low- 2hours, high- 4 hours), C-Sintering temperature (low- 1120 $^{o}$C, high- 1180$^{o}$C) ..... 33

Figure 3.1-4: Interaction effects plot of process parameters on radial shrinkage rate, A*B refers interaction between Layer thickness and Sintering time, A*C refers interaction between Layer thickness and Sintering temperature, B*C refers interaction between Sintering temperature and Sintering time ..... 34

Figure 3.1-5: Main effects plot of process parameters on longitudinal shrinkage, A-Layer thickness (low- 50 µm, high- 100 µm), B-Sintering time (low- 2hours, high- 4 hours), C-Sintering temperature (low- 1120 $^{o}$C, high- 1180$^{o}$C) ..... 35

Figure 3.1-6: Interaction effects plot of process parameters on longitudinal shrinkage rate, A*B refers interaction between Layer thickness and Sintering time, A*C refers interaction between Layer thickness and Sintering temperature, B*C refers interaction between Sintering time and Sintering temperature ..... 36

Figure 3.1-7: Percentage contributions on (a) Compressive Strength (b) Radial shrinkage rate (c) Longitudinal shrinkage rate. A-Layer thickness, B-Sintering time and C-Sintering temperature ..... 38

Figure 3.1-8: Percentage contributions on (a) Compressive Strength (b) Radial shrinkage rate (c) Longitudinal shrinkage rate. A-Layer thickness, B-Sintering time and C-Sintering temperature ..... 40

Figure 3.1-9: Percentage contributions on (a) Compressive Strength (b) Radial shrinkage rate (c) Longitudinal shrinkage rate. A-Layer thickness, B-Sintering time and C-Sintering temperature ..... 43

Figure 3.1-10: (a) Lower layer thickness showing better binder distribution, (b) Higher layer thickness showing poor binder distribution ..... 44

Figure 3.1-11: (a) Adhesion between powder particles (b) Growth of interparticle neck ..... 45

Figure 3.1-12: SEM image of sample made at Sintering time: 2 hours, temperature: 1120 $^{o}$C ... 46

Figure 3.1-13: SEM image of sample made at Sintering time: 2 hours, temperature: 1180 $^{o}$C ... 46

Figure 3.1-14: SEM image of sample made at Sintering time: 4 hours, temperature: 1120 $^{o}$C ... 46

Figure 3.1-15: SEM image of sample made at Sintering time: 4 hours, temperature: 1180 $^{o}$C ... 47

Figure 3.2-1: Training error vs number of iterations for the neural network model ..... 49

Figure 3.2-2: Performance of network architecture for different learning rates ..... 49

Figure 3.2-3: Training error vs number of iterations for the neural network model ..... 51

Figure 3.2-4: Performance of network architecture for different learning rates ..... 51

Figure 3.2-5: Training error vs number of iterations for the neural network model ..... 53

Figure 3.2-6: Performance of network architecture for different learning rates ..... 53

Figure 3.2-7: Methodology to develop own model ..... 56

Figure 3.3-1: (a) Comparison between experimental and simulation results of compression test (b) Deformation of solid analyzed in FE simulation ..... 59

Figure 3.3-2: Change in sample cross section during compression testing ..... 60

Figure 3.3-3: Load-Displacement curve comparison of simulation with experimental data. (a) Circular1, (b) Cubical 1, (c) Circular 2, (d) Cubical 2 ..... 61

Figure 3.3-4: Deformed images of FE simulation (a) Circular 1, (b) Cubical 1, (c) Circular 2 and (d) Cubical 2 ..... 61

Figure 3.3-5: Deformed images during compression testing (a) Circular 1, (b) Cubical 1, (c) Circular 2 and (d) Cubical 2. ..... 62

Figure 3.4-1: Flowchart representing the complete binder jetting process [66] ..... 64

**LIST OF TABLES**

Table 1.0-1: Additive manufacturing methods, materials, their advantages and disadvantages .... 3

Table 2.1-1: Process Parameters and Levels ..... 14

Table 2.1-2: Full Factorial Experimental Plan, Low-level is represented as 0 and High level is represented as 1. A (low- 50 µm, high- 100 µm), B (low- 2hours, high- 4 hours), C (low- 1120 $^{o}$C, high- 1180$^{o}$C) ..... 16

Table 2.1-3: Chemical composition of SS31 (wt%) ..... 16

Table 2.1-4: Formulae for Degree of freedom, Sum of squares ..... 19

Table 2.3-1: Lattice Parameters for different designs ..... 27

Table 3.1-1: Experimental results, where A: Layer Thickness, B: Sintering time and C: Sintering temperature ..... 30

Table 3.1-2: Results of Analysis of variance of compressive strength ..... 37

Table 3.1-3: Results of Analysis of variance of radial shrinkage rate ..... 37

Table 3.1-4: Results of Analysis of variance of longitudinal shrinkage rate ..... 37

Table 3.1-5: Experimental results, where A: Layer Thickness, B: Sintering time and C: Sintering temperature ..... 39

Table 3.1-6: Results of Analysis of variance for compressive strength ..... 39

Table 3.1-7: Results of Analysis of variance for radial shrinkage rate ..... 40

Table 3.1-8: Results of Analysis of variance for longitudinal shrinkage rate ..... 40

Table 3.1-9: Experimental results, where A: Layer Thickness, B: Sintering time and C: Sintering temperature ..... 41

Table 3.1-10: Results of Analysis of variance for compressive strength ..... 42

Table 3.1-11: Results of Analysis of variance for radial shrinkage rate ..... 42

Table 3.1-12: Results of Analysis of variance for longitudinal shrinkage rate ..... 42

Table 3.1-13: Optimized parameters..... 43

Table 3.2-1: Inputs A (Layer thickness), B (Sintering time), C (Sintering temperature) along with normalized output of compressive strength in the range of 0 to 1. ..... 48

Table 3.2-2: Normalized inputs and output values of circular structure..... 50

Table 3.2-3: Normalized inputs and output values of cubical structure ..... 52

Table 3.2-4: Neural network results for different structures..... 54

Table 3.2-5: Data from experimentation found in literature ..... 57

Table 3.2-6: Validation of neural network model..... 57

Table 3.3-1: Material properties used for finite element analysis. ..... 58

Table 3.3-2: Experimental and FE results..... 62

# NOMENCLATURE

| | |
|---|---|
| $A$ | Layer thickness |
| $B$ | Sintering time |
| $C$ | Sintering temperature |
| $O$ | Compressive Strength |
| $d_s$ | Diameter of sintered sample |
| $l_s$ | Length of sintered sample |
| $d_i$ | Diameter of Input CAD model |
| $l_i$ | Length of Input CAD model |
| $\bar{y}$ | Mean of all observations |
| $\bar{y}_i$ | mean of $i^{th}$ factor level of a factor |
| $\bar{y}_{ij}$ | mean of observations at the $i^{th}$ level of a factor and the $j^{th}$ level of other factor |
| $\bar{y}_{ijk}$ | mean of observations at the $i^{th}$ , $j^{th}$ , $k^{th}$ level of three factors |
| $y_{ijkl}$ | individual observation |
| $F(x)$ | Activation function |
| $\delta_j, \delta_k$ | Error information at hidden and output nodes |
| *W1, W2* | Weights at input-hidden, hidden-output nodes |
| *b1, b2* | Bias at hidden node and bias at output node |

# CHAPTER 1

## 1.0 INTRODUCTION

Additive manufacturing makes the product layer by layer according to sliced input CAD model, with very less material waste compared to conventional manufacturing. Additive manufacturing has wide range of applications which includes biomedical, automotive and aerospace industries. It has been gaining significance recently because of its ability to manufacture complex shaped geometries and low material waste compared to conventional manufacturing processes [1, 2]. The combination of additive manufacturing with topology optimization is highly desirable in many applications, one such important application is bone tissue engineering where artificial bone scaffolds are used for bone tissue regeneration. Bone scaffolds are generally made using conventional manufacturing techniques like gas foaming, solvent casting, electrospinning, freeze drying, melt molding are used for making bone scaffolds [3]. The major problem with conventional manufacturing techniques used for porous scaffolds are the control on pore sizes and interconnected pore networks. Additive manufacturing is capable of producing structures with complex internal architecture like bone scaffolds with controlled porosity, pore geometry and interconnected pore network [4]. Therefore, there is a great deal of attention to additive manufacturing technologies where three-dimensional products are made layer by layer additively according to data obtained from CAD file.

Additive manufacturing is a process of joining materials to make objects from 3D model data, usually layer upon layer, as opposed to subtractive manufacturing technology [5]. Fused deposition modeling, Selective laser sintering, Material jetting, Binder jetting, Selective laser melting are different technologies available in the market. There are many studies available in literature

regarding material property relationship studies of various additive manufacturing technologies. Fused deposition modeling (FDM) is a material extrusion process used to make thermoplastic parts through heated extrusion and deposition of materials layer by layer [6]. Priyank et al. studied the effect of process parameters on tensile and compressive properties of polylactic acid (PLA) specimens made using fused deposition modeling [7]. Godfrey et al. studied the influence of fused deposition modeling process parameters on mechanical properties of Acrylonitrile butadiene styrene samples [8]. Jaya et al. studied the influence of process parameters on the mechanical properties of 3D printed Acrylonitrile butadiene styrene (ABS) and hydrous magnesium silicate composite made using fused deposition modeling [9]. Selective laser sintering (SLS) uses laser to melt and solidify layers of powder, the laser selectively sinters the powder material [10]. It is widely used technology in industry for making functional prototypes. Ruban et al. studied the effect of process parameters on mechanical properties of stainless steel samples fabricated using selective laser sintering [11]. Z.H Liu and Jie Liu et al. studied the process-property relationship of selective laser sintering of ceramic materials [12, 13]. Andreas and Eva et al. studied the correlation of process parameters with mechanical properties of selective laser sintered polymer materials [14, 15]. Material jetting technology is similar to that of 2D printing but instead of jetting drops on ink onto the paper, it jets liquid photopolymer onto the build plate and cures it using UV light. Kampker et al. studied the material and parameter analysis of polyjet process using design of experiments [16]. Kesy et al. investigated the mechanical properties of parts produced by using polymer jetting technology [17]. Additive manufacturing technologies and the materials it uses to fabricate the products are listed in Table 1. It also outlines the main advantages and disadvantages of each technology, as reviewed from the literature [18, 19].

Table 1.0-1: Additive manufacturing methods, materials, their advantages and disadvantages

| Additive Manufacturing | Materials | Advantages | Disadvantages |
|---|---|---|---|
| **Powder-based Three-dimensional printing** | ➢ Composites<br>➢ Polymers<br>➢ Ceramics<br>➢ Calcium phosphate | ➢ Wide range of material choice | ➢ Lower green part strength |
| **Selective laser sintering** | ➢ Polymers<br>➢ Ceramics | ➢ No post processing required<br>➢ Better mechanical properties | ➢ Slow process and expensive |
| **Fused Deposition Modeling** | ➢ Thermoplastics | ➢ Fast and inexpensive | ➢ Less material choices |
| **Stereo lithography** | ➢ Polymers | ➢ Better resolution | ➢ Applicable only to photopolymers |

Binder jet additive manufacturing has the ability to fabricate complex geometrical parts with no support structures, the important advantage is that it doesn't employ heat during part building process where most of the additive manufacturing technologies employ heat in building stages which can create residual stresses in the parts. Also, surface finish of the parts manufactured using binder jetting are significantly better than that of other additive manufacturing processes [20]. The above advantages of binder jetting make it best fit for use in biomedical applications.

Binder jet additive manufacturing technology is originally developed at MIT in 1990 and commercialized in 2010 [19]. This technology is capable of printing variety of materials including metals, sand, and ceramics. Binder jetting is an additive manufacturing process in which liquid binding agent is selectively deposited on powder particles. The print head strategically drops binder into powder and layers are then bonded together to form 3D product. The process involves

binding, curing, de-powdering, sintering, and finishing. The schematic representation of binder jetting is shown in Figure 1.0-1 and the main technique of manufacturing using binder jet additive manufacturing is as follows. (a) The CAD file is sliced into layers and STL file is generated, (b) Each layer begins with thin distribution of powder spread over the surface of a powder bed, (c) Using a technology similar to ink-jet printing, a binder material selectively joins particles where the object has to be formed, (d) A piston that supports the powder bed and part in progress lowers so that the next powder layer can be spread and selectively joined, (e) This layer by layer process repeats until the part is completed. (f) Following a heat treatment, unbound powder is removed and the metal powder is sintered together.

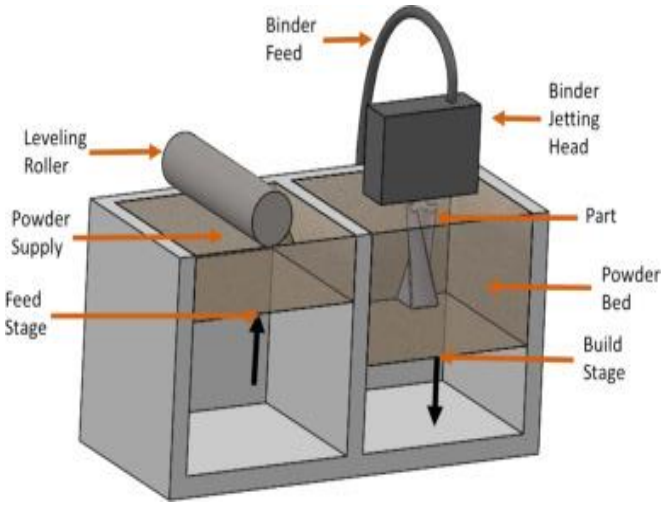


Figure 1.0-1: Schematic representation of binder jetting process *[21]*

Binder jet additive manufacturing consists of following main processes mainly printing, curing, de-powdering, sintering, and finishing. The printing process is followed by curing where the samples from printer are transferred to preheated oven. Once curing is done, samples are transferred to sintering furnace where samples are sintered at specific temperature and time in controlled atmosphere. The final step after sintering is to post-process the samples based on the purpose.

The process parameters which effects the output characteristics of samples are represented in fish-bone diagram as shown in Figure 1.0-2. The parameters include powder size, layer thickness during binding, part orientation in the bed, drying time during binding, heater power, roller speed, curing temperature, curing time, sintering time, sintering temperature and sintering atmosphere. Any variation in the above-mentioned parameter changes the output properties. Similar to conventional manufacturing, there are many process parameters to be set before manufacturing. Binder jetting involves lot of processes involved which makes the relationship between input process parameters and output properties very complicated. Hence there is a need to tune the process parameters to achieve controlled and stable process.

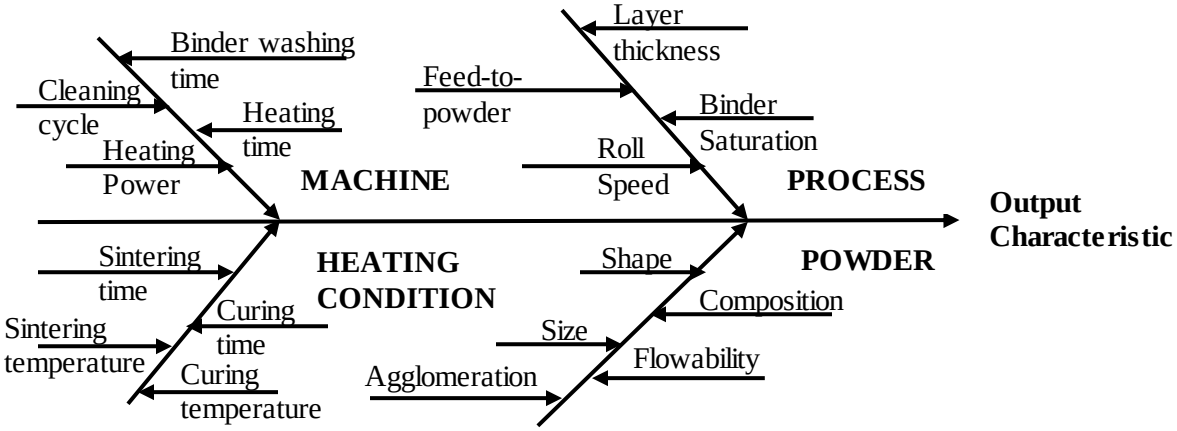


Figure 1.0-2: Fishbone diagram representing various parameters involved in the process

Few researchers studied the relationship between process parameters and output characteristics obtained using binder jet additive manufacturing technology. Yao et al. investigated the process parameters including binder setting saturation value, layer thickness, location of made up parts for ZCorp 3D printing system with plaster powder and identified the process parameters to reduce the building time [22]. Vaezi et al. studied the influence of binder saturation and layer thickness on mechanical strength, surface quality of plaster-based powder and found that the uniform layer thickness and increase in binder saturation resulted in increased tensile and flexural strength with

low dimensional accuracy [23]. Hsu et al. studied the influence of layer thickness, binder saturation, location of green parts, powder type and optimized the parameters for ZCorp 3D printing improving dimensional accuracy, less fabrication time and less binder consumption [24]. Shresta et al. studied the effect of binder saturation, layer thickness, roll speed, feed-to-powder ratio on transverse rupture strength and found that binder saturation and feed-to-powder ratio are most critical factors influencing mechanical properties [25]. Suwanprateeb et al. studied the influence of layer thickness and binder saturation on transformation efficiency of 3D printed plaster of paris and found that low layer thickness, saturation yielded high transformation efficiency [26]. Chen et al. studied the influence of layer thickness, drying time, binder saturation on dimensional accuracy and surface finish of SS420 sample and found that layer thickness, binder saturation influenced surface finish whereas dimensional accuracy is influenced by drying time [27]. Tang et al. study was focused on mechanical properties of SS316 samples made by binder jetting with default process parameters [28]. Bai et al. studied the effect of powder size and sintering atmospheric control on part density, shrinkage and found that controlled sintering atmosphere in with presence of hydrogen improves the sintered density of copper samples [29]. Doyle et al. studied the effect of layer thickness and orientation on mechanical behavior of stainless steel bronze parts made using binder jetting and found that layer thickness as larger influence than orientation on tensile mechanical properties of bronze infiltrated stainless steel samples [30].

Most of the researchers studied the binder jetting of polymer materials and there are very few studies on the optimization of process parameters for binder jet additive manufacturing of metal parts. Also, most of the studies considered printing setup parameters like powder size, binder saturation, layer thickness, and drying time leaving behind the heat treatment parameters effect. Hence, there is a need to carry out optimization studies involving metal manufacturing and the

current research is carried out to study the effect of printing setup parameter layer thickness in combination with sintering parameters, temperature and time. Output characteristics considered are compressive strength, radial, and longitudinal shrinkage rates, these are chosen from the binder jetting application perspective in bone scaffold engineering, as the complex bone structure produced should be dimensionally accurate with compressive strength.

Apart from studying the process property relationship, it is very important to establish quantitative relationship between process parameters and properties, as it cuts down the cost of experiments. Physics-based modelling is almost impossible for 3D printing, as it involves powder-binder reaction, curing and sintering. Hence numerical models can be effective in finding the appropriate parameters with respect to desired output characteristics. Artificial neural network is the well-known method to serve as a numerical model based on experimental data, hence a numerical model can be developed for the 3D printing process using artificial neural network. Figure 1.0-3 shows the schematic representation of neural network generating output values based on fed input parameters. Applications of artificial neural network include thin films & superconductors, materials, machining & processing, thermal and mechanical fields [31]. Neural networks are found to be best in constructing complex map between inputs and output of a system. It is a system of mathematical equations working on data approximating the human brain. Neural network consists of neurons connecting each other with respective weights and passing the information. Awodele et al. defined artificial neural network as brain in aspect that knowledge is gained through learning and weights are used to store the knowledge [32].

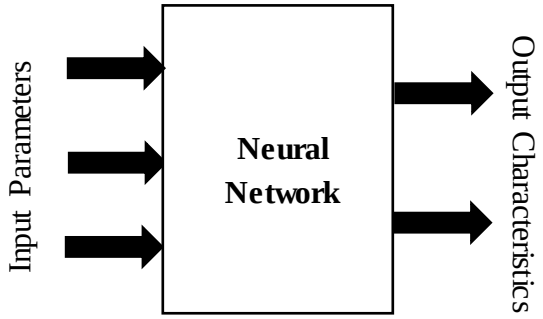


Figure 1.0-3: Neural Network Schematic representation

Cundari et al. compared neural network models to quantum mechanical models for predicting the mechanical properties of inorganic system and concluded that neural networks give more accurate predictions [33]. Asada et al. used feedforward backpropagation network to predict the superconducting transition temperature of material as a function of chemical composition [34]. Vermeulen et al. used feed-forward back propagation neural network to predict the finishing temperature of rolling mill as a function of processing parameters [35]. Al-Assaf et al. used multilayer feed forward neural network to predict the fatigue life of unidirectional composite [36]. Scott et al. designed an artificial neural network to predict the properties of ceramic materials as a function of material composition [37]. Bilal et al. used the artificial neural network to predict the hardness of aluminum alloys [38].

Very few studies are done on neural network modelling of additive manufacturing processes. The current research aims at developing a predictive model using feed forward back propagation artificial neural network. Neural network has been used in manufacturing industry but only few researchers used artificial intelligence algorithms for additive manufacturing process. Asadi et al. implemented particle swarm optimization algorithm to the obtain the optimum topology of aggregate artificial neural network with layer thickness, delay time between spreading layers, print orientation as input parameters and compressive strength as output parameters [39]. Georgios et

al. used the neural network models to assess the quality characteristics of printed electronic products caused by dimensional deviations [40].

Additive Manufacturing can process more complex structures compared to conventional manufacturing, a good example is lattice structures. Even with the numerous applications of lattice structures, there is still a manufacturing complexity. Casting, brazing, metal forming are the manufacturing techniques used for making simple lattice structures, the structures made by these techniques has limited design freedom. Additive Manufacturing can be used to make cellular structures of complex designs, it is found to be promising technology to produce lattice structures with controlled porosity and pore size. Metal cellular structures exhibit a combination of high-performance characteristics as high strength, low mass, good energy absorption and thermal properties [41, 42]. Cellular structures can be classified based on the topology of the pore and cell size. Metal stochastic cellular structures and periodic lattice cellular structures are two types of cellular structures. Metal stochastic cellular structures typically have a random distribution of open or closed voids and metal periodic cellular lattice structures have uniform structures that are generated by repeating a unit cell. Periodic lattice structures have superior mechanical properties than that of stochastic metal structures, structural performance of lattice strut structures with less than 5% density was proven to be up to three times higher than that of stochastic foams [43, 44]. Hence metal lattice structures are of greater interest to study and the most relevant applications of lattice structures are found in the fields of biomedical, aerospace, chemical and automotive industries.

Lot of research has been conducted regarding the application of additive manufacturing in making cellular structures. Osman et al. studied the compressive properties of cellular lattice structures manufactured using fused deposition modeling [45]. Mullen et al. developed an approach based

on a defined regular unit cell to design and produced structures using selective laser sintering with a large range of both physical and mechanical properties [46]. Chunze et al. studied the performance of stainless steel lattice cellular structure fabricated via selective laser sintering technique [47]. Contuzzi et al. investigated compressive property of Ti6Al4V pillar textile unit cell made by selective laser melting [48]. Seyed et al. studied the mechanical properties of porous biomaterials made from six different space-filling units are studied [49]. Farzadi et al. studied the compressive properties of lattice structure made using powder-based inkjet 3D printing [50]. Recep et al. studied design, optimization, and evaluation of periodic lattice-based cellular structures fabricated by additive manufacturing [51]. Christiane et al. conducted the experimental analysis of additive manufactured parts with diverse unit cell structures in compression and flexural tests [52]. Mechanical testing shows that the additively made produced material is highly anisotropic and that the material has many advantages compared to the traditionally manufactured [53].

Large amount of research is dedicated on manufacturing of lattice structures using additive manufacturing and very few studies deals with finite element simulation of lattice structures fabricated using additive manufacturing. Jie et al. performed finite element analysis to evaluate the mechanical properties of cellular structures [54]. Mark et al. validated the finite element simulation of cellular structures with empirical data obtained from compression testing of samples made using selective laser sintering [55]. Uzoma et al. developed the finite element model to simulate the compressive behavior and compared it with experimental results [56]. Clayto et al. simulated the diamond lattice structures of different unit sizes and compared it with experimentation results [57]. Kolan et al. performed finite element analysis to predict the compressive behavior of five different porous structures made using selective laser sintering [58]. Langranda et al. investigated the

influence of element type and numerical scheme on structural response of cellular materials under compressive load [59]. There is a need to develop the finite element models of binder jet additively manufactured lattice structures as it eliminates the need for experiments cutting down the experimentation cost and time. The current study also explores the compressive behavior of lattice structures by simulating the finite element model developed from experimental compression data of solid cylinder along with performing process-parameter optimization.

## 1.1 RESEARCH OBJECTIVES AND SCOPE

The main objective of the study is to optimize process parameters of binder jet additive manufacturing for producing quality products. The study aims at the understanding the relationship between printing parameters and printing accuracy along with compressive strength. Three important parameters layer thickness, sintering time and sintering temperature were identified for the study and full factorial experimental design is used to conduct experiments for determining the relationship between process parameters and mechanical properties namely compressive strength, radial, and longitudinal shrinkage rates. Effect plots are used to visualize the impact of each parameter combination and to identify the most influential parameters. The significance of each parameter is determined based on analysis of variance from experimental data obtained from compression testing the samples.

Also, a predictive model is designed to define the relationship between process parameters and compressive strength using the experimental data. Feedforward back propagation neural network was used to develop predictive model which establishes the relationship between process parameters and desired output characteristics. Finally, a finite element model was developed using the experimental data obtained from compression test and used as input to simulate the compressive behavior of four different lattice designs. The model was validated by comparing the

FE simulation results with that of experimental compression test results of different lattice structures.

# CHAPTER 2

## 2.0 PROCESS AND APPROACHES

The current study is divided into two different parts, first of all experimentation is performed to study the effect of process parameters on compressive strength, shrinkage rate and secondly, numerical modelling is done using artificial intelligence approach to develop a prediction model and also finite element modelling is carried out using the experimental data.

## 2.1 EXPERIMENTAL METHOD AND DESIGN

The experimental methodology followed in the study is shown in Figure 2.1-1. The study starts with selecting the parameters for the study, followed by creating an experimental plan using design of experiments to fabricate the samples. The fabricated samples are tested for its mechanical properties and the data obtained from experiments are analyzed to understand the effect of build parameters.

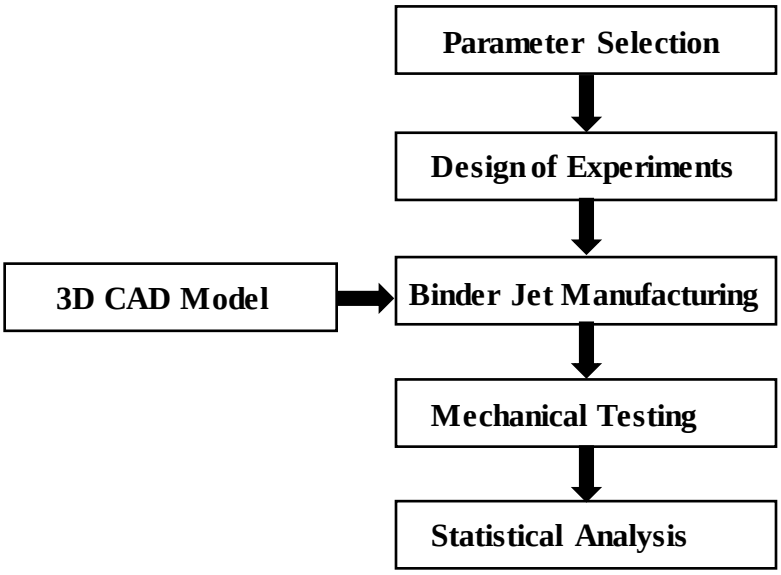


Figure 2.1-1: Flow Diagram of Experimental Methodology

Design of experiments approach was used to determine the influence the effect of input parameters on output characteristics. Full factorial design of experiments approach was used to conduct the experiments in this research, where all the combinations of process parameters were considered. In this study, as mentioned earlier three important factors namely layer thickness, sintering time and sintering temperature were considered with two levels. Table 2.1-1 lists the factors considered along with their levels and ranges. It also lists material and the machine used to fabricate the sample.

Table 2.1-1: Process Parameters and Levels

| **Factor** | **Level 1(0)-low** | **Level2(1)-high** |
|---|---|---|
| **Layer thickness(A), µm** | 50 | 100 |
| **Sintering time(B), hours** | 2 | 4 |
| **Sintering temperature(C), ºC** | 1120 | 1180 |
| **Material:** SS 316 | | |
| **Machine:** ExOne M-lab 3D printer | | |

ExOne M-lab machine used for fabricating samples along with highlighting binding agent, cleaning agent, and waste collector are shown in Figure 2.1-2a. Layer thickness (A), Sintering time (B), Sintering temperature (C) are the input parameters considered. Ideal product will be one of high compressive strength with low shrinkage in radial and longitudinal directions of sample, low shrinkage means the dimensions of sample are close enough to CAD model dimensions. Radial shrinkage and longitudinal shrinkage directions are represented in Figure 2.1-2b. Radial shrinkage refers to dimension change in radius of sample and radius of input CAD model, whereas longitudinal shrinkage refers to dimensional change in length of sample and length of input CAD model.

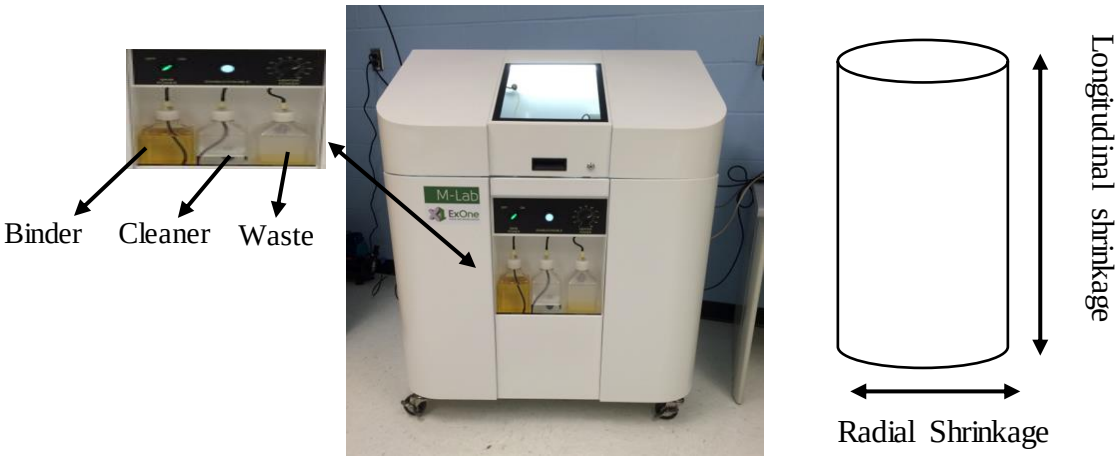


Figure 2.1-2: (a) ExOne M-lab machine, (b) Radial shrinkage and longitudinal shrinkage directions

### 2.1.1 Full Factorial Design of Experiments

Full factorial design of experiments was used to test all the possible combinations in current research with three parameters and two levels each, $2^3$ =8 experiments should be conducted. Table 2.1-2 represents the total experiments considered in the study. The experimental plan in Table 2.1-2 was used to produce the parts for study and two samples are fabricated in each experimental run. Example, experimental number 5 represents the settings of Layer thickness: 100 µm (high), Sintering time: 2 hours (low) and Sintering temperature: 1120 $^{o}$C (low). All the eight experiments will be run and the desired output characteristics compressive strength, radial shrinkage and longitudinal shrinkage will be reported.

Table 2.1-2: Full Factorial Experimental Plan, Low-level is represented as 0 and High level is represented as 1. A (low- 50 µm, high- 100 µm), B (low- 2hours, high- 4 hours), C (low- 1120 $^{o}$C, high- 1180$^{o}$C)

| **Experiment** | **Layer Thickness(A)** | **Sintering Time(B)** | **Sintering Temperature(C)** |
|---|---|---|---|
| 1 | 0 | 0 | 0 |
| 2 | 0 | 0 | 1 |
| 3 | 0 | 1 | 0 |
| 4 | 0 | 1 | 1 |
| 5 | 1 | 0 | 0 |
| 6 | 1 | 0 | 1 |
| 7 | 1 | 1 | 0 |
| 8 | 1 | 1 | 1 |

#### 2.1.1.1 Material

The powder material used is Stainless steel 316 powder with particle size of 30 µm, the material is obtained from Ex-One and used with no further treatment. The chemical composition of stainless steel powder is showed in the Table 2.1-3.

Table 2.1-3: Chemical composition of SS31 (wt%)

| **C** | **Mn** | **P** | **S** | **Si** | **Cr** |
|---|---|---|---|---|---|
| 0.08 max | 2.00 max | 0.045 max | 0.03 max | 0.75 max | 16.00-18.00 |

### 2.1.2 Sample Preparation

The sample used in the study are cylindrical structures with dimensions 25mm length and 10 mm diameter, the CAD model is designed in Creo 3.0. Then the CAD model is sliced to layers and the generated STL model is input to system for printing. The 3D printing process starts with loading the powder material into the bed. Along with powder material, the STL file has to be uploaded into the system and the sample fabricated is shown in Figure 2.1-3.

Figure 2.1-3: Binder jet additive manufactured solid cylindrical sample

### 2.1.3 Compression Testing

Compression testing was carried out on samples according to ASTM E9 standards for metallic materials [60]. MTS 810 material testing system with a 1 KN load cell at a constant crosshead speed of 0.1 in/ min was used and the data recorded for every 0.05 seconds, shown in Figure 2.1-4. The stress-strain curves were derived from the load-displacement data obtained during experiments. Figure 2.1-4 shows the sample in between the compression platens of MTS machine during the testing.


Figure 2.1-4: Sample in between compression platens of MTS Machine

### 2.1.4 Main and Interaction Effect plots

Main effects plot graphically displays the average value of output for multiple levels of given single input. The plot helps us to visualize the magnitude and direction of change in output with change in the value of input factor.

Interaction effects plot graphically displays the average value of output for multiple levels of two inputs. Interaction effects plot helps us to visualize the magnitude and direction of change in output with change in the values of two input factors.

Main effect is calculated by differencing the average of factor and grand mean at each factor level and the interaction effect is calculated by averaging the response of each level combinations of two factors at a time. The main effects and interaction effects of process parameters on output characteristics are obtained from the experimental results and are plotted below.

### 2.1.5 Analysis of Variance

Table 2.1-4 represents the calculations needed to perform analysis of variance on compressive strength, longitudinal shrinkage and radial shrinkage rates. The percentage contribution of each

factor layer thickness, sintering time and sintering temperature on compressive strength, radial shrinkage rate and longitudinal shrinkage rate was calculated. The results of analysis of variance of factors on output characteristics were calculated using Minitab software and are presented in following sections.

Table 2.1-4: Formulae for Degree of freedom, Sum of squares

| Factor | DF (Degree of Freedom) | SS (Sum of Squares) |
|---|---|---|
| **A** | a-1 | $\sum_{i=1}^{a}(\bar{y}_i - \bar{y})^2$ |
| **B** | b-1 | $\sum_{j=1}^{b}(\bar{y}_j - \bar{y})^2$ |
| **C** | c-1 | $\sum_{k=1}^{c}(\bar{y}_k - \bar{y})^2$ |
| **AB** | (a-1) (b-1) | $\sum_{j=1}^{b}\sum_{i=1}^{a}(\bar{y}_{ij} - \bar{y}_i - \bar{y}_j + \bar{y})^2$ |
| **AC** | (a-1) (c-1) | $\sum_{k=1}^{c}\sum_{i=1}^{a}(\bar{y}_{ik} - \bar{y}_i - \bar{y}_k + \bar{y})^2$ |
| **BC** | (b-1) (c-1) | $\sum_{j=1}^{c}\sum_{k=1}^{b}(\bar{y}_{kj} - \bar{y}_i - \bar{y}_j + \bar{y})^2$ |
| **ABC** | (a-1) (b-1) (c-1) | $\sum_{k=1}^{c}\sum_{j=1}^{b}\sum_{i=1}^{a}(\bar{y}_{ijk} - \bar{y}_{ij} - \bar{y}_{ik} - \bar{y}_{jk} + \bar{y}_i + \bar{y}_j + \bar{y}_k - \bar{y})^2$ |
| **Error** | abc (n-1) | $\sum_{l=1}^{n}\sum_{k=1}^{c}\sum_{j=1}^{b}\sum_{i=1}^{a}(y_{ijkl} - \bar{y}_{ijk})^2$ |
| **Total** | abcn-1 | $\sum_{l=1}^{n}\sum_{k=1}^{c}\sum_{j=1}^{b}\sum_{i=1}^{a}(y_{ijkl} - \bar{y})^2$ |

Where,

a: number of levels in factor A, where A: Layer thickness, a=2 (low level, high level)

b: number of levels in factor B, where B: Sintering time, b=2 (low level, high level)

c: number of levels in factor C, where C: Sintering temperature, c=2 (low level, high level)

n: number of observations

$\bar{y}$ : mean of all observations

$\bar{y}_i$ : mean of $i^{th}$ factor level of factor A

$\bar{y}_j$ : mean of $j^{th}$ factor level of factor A

$\bar{y}_k$ : mean of $k^{th}$ factor level of factor A

$\bar{y}_{ij}$ : mean of observations at the $i^{th}$ level of factor A and the $j^{th}$ level of factor B

$\bar{y}_{ik}$ : mean of observations at the $i^{th}$ level of factor A and the $k^{th}$ level of factor C

$\bar{y}_{kj}$ : mean of observations at the $k^{th}$ level of factor C and the $j^{th}$ level of factor B

$\bar{y}_{ijk}$ : mean of observations at the $i^{th}$ level of factor A, $j^{th}$ level of factor B and $k^{th}$ level of factor C

$y_{ijkl}$ : individual observation

MS (Mean Squares) = SS (Sum of Squares)/DF (Degree of freedom)

F-Value= MS of Factor/MS of Error

## 2.2 NEURAL NETWORK MODEL

Artificial neural networks are best tools compared to other available data modelling tools, as it is capable of mapping complex non-linear relationship between input factors and output characteristics. After training the neural network with known data, it is capable of providing approximate output results with unseen data which makes the technique useful for predictive applications. Feedforward back propagation neural network is the simplest ANN in use and found its applications in developing predictive experimental models. Feed forward back propagation neural network with sigmoid activation function was considered for designing the experimental model. There are three different layers in neural network.

Input layer: The leftmost layer, input parameters are feed into neural network through this layer. Hidden layer: The layer connecting the input and output layer is hidden layer, it is called hidden as its values are not observed in the training set.

Output layer: The rightmost layer, where all the hidden neurons produce output.

Figure 2.2-1 represents the architecture of neural network used in the study. In feed forward, neurons in input layer are connected to neurons in hidden layer, whereas neurons in hidden layer are connected to output layer. Backpropagation is a training method in which neurons adjust their weight to achieve the target output. The network contains three layers with a total of 8 nodes, 4 being hidden nodes, 3 input nodes and 1 output node.

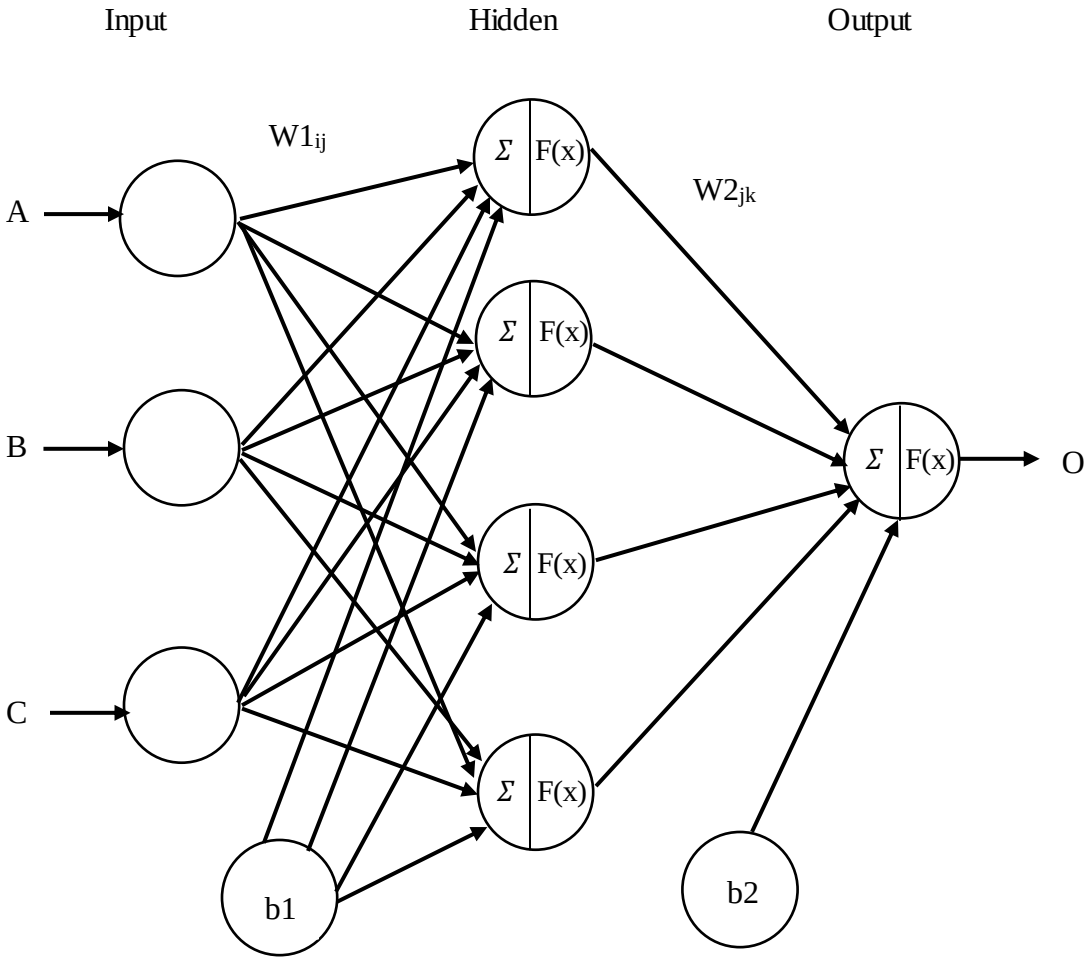


Figure 2.2-1: Neural Network Schematic representation, Where A-Layer thickness, B-Sintering time, C-Sintering temperature, O-Compressive Strength, Σ represents summation & F(x) is activation function, b1 & b2 are bias

Xi – Input values fed to neural network through input node i

$W1_{ij}$- Weights connecting input-hidden nodes where i represents input node and j represents hidden node

$W2_{jk}$- Weights connecting hidden-output nodes where j represents hidden node and k represents output node

b1- Bias at hidden node

b2-Bias at output node

F(x) - Activation function

$\delta_k$-Error information at output node

$\delta_j$-Error information at hidden node

ΔW1- Delta weights at input-hidden layer

ΔW2- Delta weights at hidden-output layer

$Z_j$ – Hidden node, $Y_k$– Output node

Sigmoid function is used as activation function for this model

F(x) =1/(1+e^(-x))

Training Procedure:

Feedforward

1. Random numbered weights for input-hidden layer and hidden-output layer are initialized
2. The inputs are transferred to nodes in hidden layer where the summation of input values with respective node weights take place and then transferred to next layer applying the activation function

$$Z_{in}=\sum X_i * W1_{ij} + b1_i \quad (1)$$

$$Y_{in}=F(Z_{in}) \quad (2)$$

3. The values at hidden nodes gets transferred to output nodes where it gets multiplies with respective weights before applying activation function to produce output

$$Y_{out}=\sum Y_{in} * W2_{jk}+b2_j \quad (3)$$

$$Output=F(Y_{out}) \quad (4)$$

Back Propagation:

4. The error or margin is calculated by comparing target value with output value of the developed model

$$e= (Target-Output)^{2} \quad (5)$$

5. Error information at output unit is

$$\delta_k = e * F'(Y_{out}) \quad (6)$$

6. Error information at hidden unit is

$$\delta_j = F'(Z_{in}) * \sum_k \delta_k W2_{jk} \quad (7)$$

7. Weights updation at input-hidden layer

$$\Delta W1=\delta_k Y_{in} \quad (8)$$

$$(W1)_{new} = (W1)_{old}+\Delta W1 \quad (9)$$

8. Weights updation at hidden-output layer

$$\Delta W2=\delta_j X_i \quad (10)$$

$$(W2)_{new} = (W2)_{old}+\Delta W2 \quad (11)$$

The compressive strength value is normalized so all the values are in the range of 0 to 1 using the formula

$$O_i = \frac{Y_i - \min(Y)}{\max(Y) - \min(Y)} \quad (12)$$

Where $Y_i$ represents compressive strengths of each experimental run $i$ (1 to 8)

The training process and parameters involved at each step are shown in Figure 2.2-2. The neural network is trained such that error between desired output and actual output is less than 0.05.

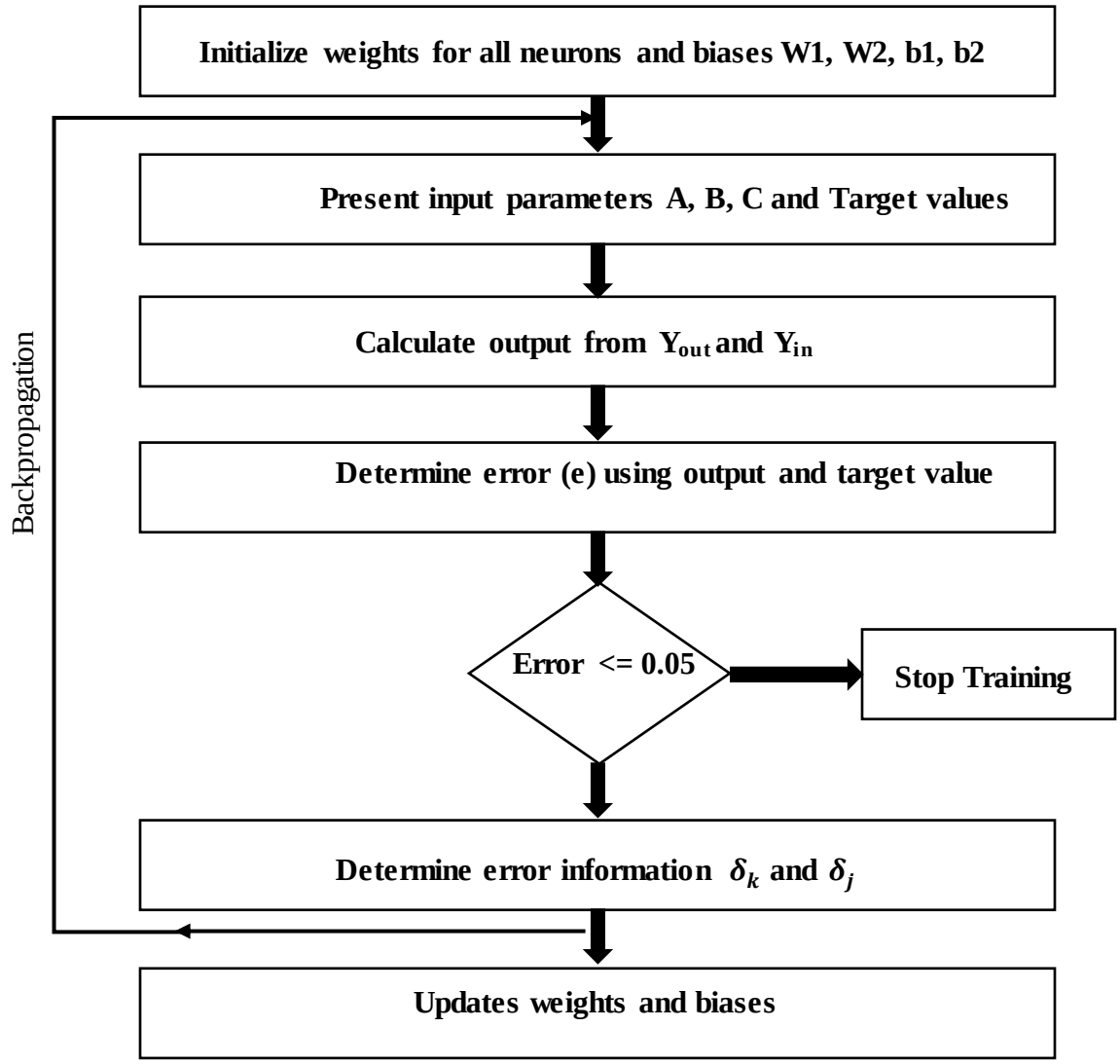


Figure 2.2-2: Flow chart showing the entire training process and the parameters involved.

After successful training, the network is tested with new data sets for its performance. Then the value obtained using the network is denormalized to find the difference between the predicted value and actual value.

$$Y_{predicted} = [Y_{network\ value} * (\max(Y) - \min(Y))] + \min(Y) \quad (13)$$

## 2.3 FINITE ELEMENT MODELLING

The methodology followed in simulating the compressive behavior of binder jet made samples was shown in Figure 2.3-1, the material model is developed from compression test data, different designs were used as input geometry and the ANSYS model is set up with appropriate boundary conditions for simulation.

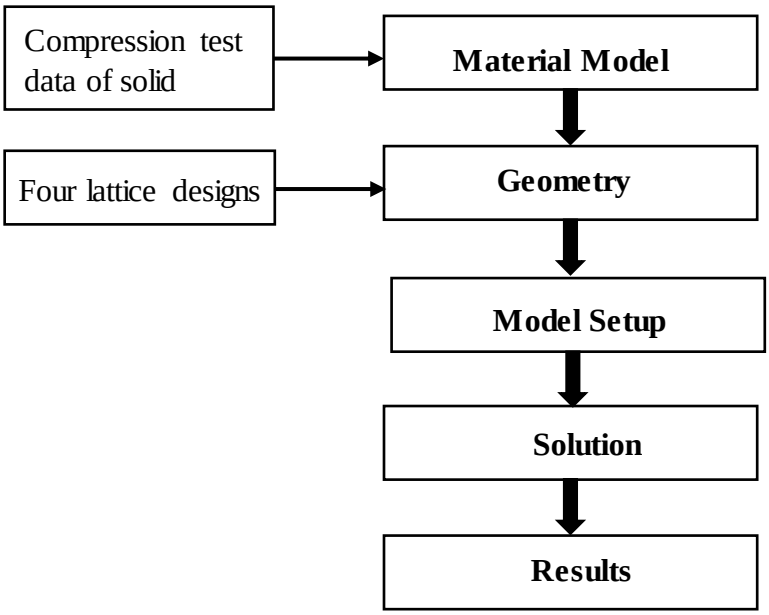


Figure 2.3-1: Finite element Analysis Methodology

### 2.3.1 Designs

In biomedical industry, pore size and shape is of great interest as it plays an important role in bone tissue regeneration [58]. Four different lattice designs of length 25 mm and diameter 10mm are

considered in the study and size of unit cells are 1000 µm and 2000 µm with cubical and circular architecture. Pore sizes are chosen in accordance with the previous studies. Farzadi et al. investigated 3D printed calcium sulfate based porous structures of pore sizes 400 µm, 600 µm, 800 µm for use in bone tissue engineering [50]. Kolan et al. studied bioactive glass porous structures of pore sizes 1000 µm and 2000 µm for use in bone tissue engineering [61]. Table 2.3-1 shows the details of all four designs used in the study and Figure 2.3-2 represents the CAD models of unit cells and lattice designs used in study.

Table 2.3-1: Lattice Parameters for different designs

| **Name** | **Geometry** | **Size(µm)** | **Gap b/w cells(µm)** | **Surface Area ($mm^2$)** | **Volume ($mm^3$)** | **Porosity (%)** |
|---|---|---|---|---|---|---|
| **Cubical1** | Cubical | 1000 | 1000 | 69.53 | 1314.55 | 35 |
| **Circular1** | Circular | 1000 | 1000 | 71.47 | 1438.08 | 25 |
| **Cubical2** | Cubical | 2000 | 1500 | 62.53 | 971.52 | 50 |
| **Circular2** | Circular | 2000 | 1500 | 65.97 | 1147.54 | 40 |

With above parameters, four lattice designs were created using Creo Parametric 3.0.

(a) (b) (c) (d) (e) (f)

Figure 2.3-2:(a) Cubical unit cell (b) Circular unit cell (c) Circular 1 (d) Cubical 1 (e) Circular 2 (f) Cubical 2

### 2.3.2 Material Properties

Stainless Steel 316 powder was used for creating all the samples and the parameters used for manufacturing is layer thickness of 100 µm and sintered at temperature of 1120°C and for a

duration of 2 hours. Various lattice structures fabricated are shown in Figure 2.3-3. MTS testing machine was used to carry out compression testing on four designs at same compression rate, 0.1 in/min and same conditions according to ASTM E9-09 standards.

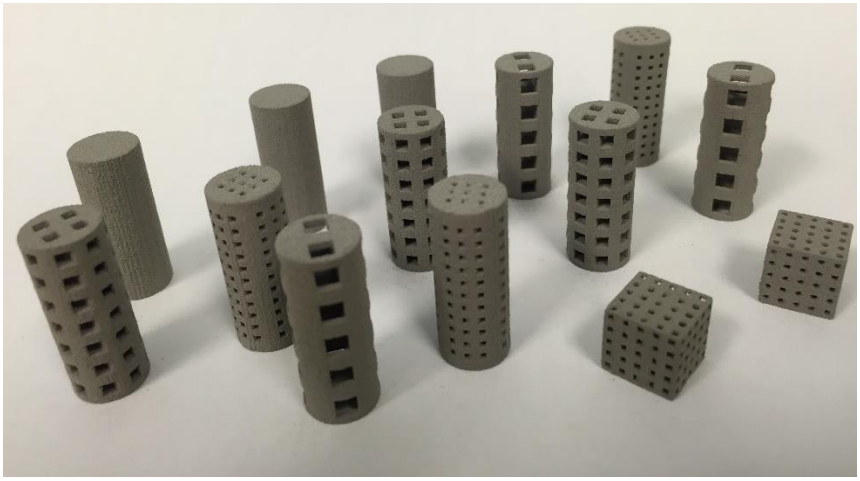

Figure 2.3-3: Binder jetting fabricated samples of various lattice structures

Finite element analysis is done for compression test of four lattice configurations, the material properties of stainless steel were assigned in ANSYS according to experimental data obtained from compression testing of solid cylinder at same experimental conditions.

The material properties were derived from the physical testing of solid stainless-steel cylinder, the samples were compressed and experimental stress-strain curve was used as input to create the material model. A linear elastic along with multilinear isotropic plasticity model were assigned to the model with the Young's modulus of 2508.4 Mpa and Poisson's ratio of 0.3. The ultimate compressive stress value assigned is 743.3 Mpa at a plastic strain of 0.36 which is obtained from the experimental stress-strain curve. The lower surface of the lattice designs is fixed and the displacement rate is applied on opposite surface to imitate the experimental setup. The simulation was carried out for all the designs with same material model, same boundary conditions and the results are presented in following sections.

# CHAPTER 3

## 3.0 RESULTS AND DISCUSSION

Experimental analysis was performed to determine the effect and significance of layer thickness, sintering time and sintering temperature on compressive strength, shrinkage rates. The same experimental data was used to develop the model predicting compressive strength given the inputs of layer thickness, sintering time and temperature. Finally, finite element simulation results were compared with that of actual experimental results for four lattice structures considered in the study.

## 3.1 EXPERIMENTAL ANALYSIS: EFFECT OF BUILD PARAMETERS

Experiments were conducted according to full factorial design of experiments plan as discussed in the last chapter. The length and diameter of each sample was recorded after sintering to get shrinkage rate in radial and longitudinal directions and are calculated as below.

$$Radial\ Shrinkage(\%) = \frac{d_s - d_i}{d_u} * 100$$

$$Longitudinal\ Shrinkage(\%) = \frac{l_s - l_i}{l_u} * 100$$

Where $d_s$, $d_i$ are diameters of sintered sample and input CAD model

$l_s$, $l_i$ are diameters of sintered sample and input CAD model

Along with shrinkage rates, ultimate compressive strength is also the output characteristic to be studied. The load-displacement data from compression test were converted to stress-strain values, the ultimate compressive strength is then obtained from stress-strain data.

$$Compressive\ Strength(Mpa) = \frac{Compressive\ Load}{Cross\ sectional\ Area}$$

### 3.1.1 Solid Structure

The compressive strength, radial and longitudinal shrinkage for solid samples made with different experimental settings were calculated and tabulated below. The experimental results from Table 3.1-1 were analyzed to find the effects of build parameters.

Table 3.1-1: Experimental results, where A: Layer Thickness, B: Sintering time and C: Sintering temperature

| # | A | B | C | Compressive Strength(Mpa) | Radial Shrinkage (%) | Longitudinal Shrinkage (%) |
|---|---|---|---|---|---|---|
| 1 | 0 | 0 | 0 | 745.5 | 0.3 | 1.5 |
| 2 | 0 | 0 | 1 | 1780.5 | 1.9 | 2.3 |
| 3 | 0 | 1 | 0 | 1811 | 2.9 | 2.5 |
| 4 | 0 | 1 | 1 | 1972 | 3.7 | 2.6 |
| 5 | 1 | 0 | 0 | 82.89 | 0.0 | -0.1 |
| 6 | 1 | 0 | 1 | 879.5 | 2.7 | 1.8 |
| 7 | 1 | 1 | 0 | 978.5 | 2.3 | 2.0 |
| 8 | 1 | 1 | 1 | 1083.5 | 2.5 | 2.9 |

The effect of different parameters on compressive strength of binder jet made solid samples are shown in Figure 3.1-1. The effects plot reveals that all the three parameters are significant and compressive strength is high for sample fabricated with low layer thickness, long sintering time and higher sintering temperature. It means lower layer thickness produced sample with high compressive strength than higher layer thickness, long sintering time produced sample with high compressive strength than lower sintering time, higher sintering temperature produced sample with higher compressive strength than lower sintering temperature.

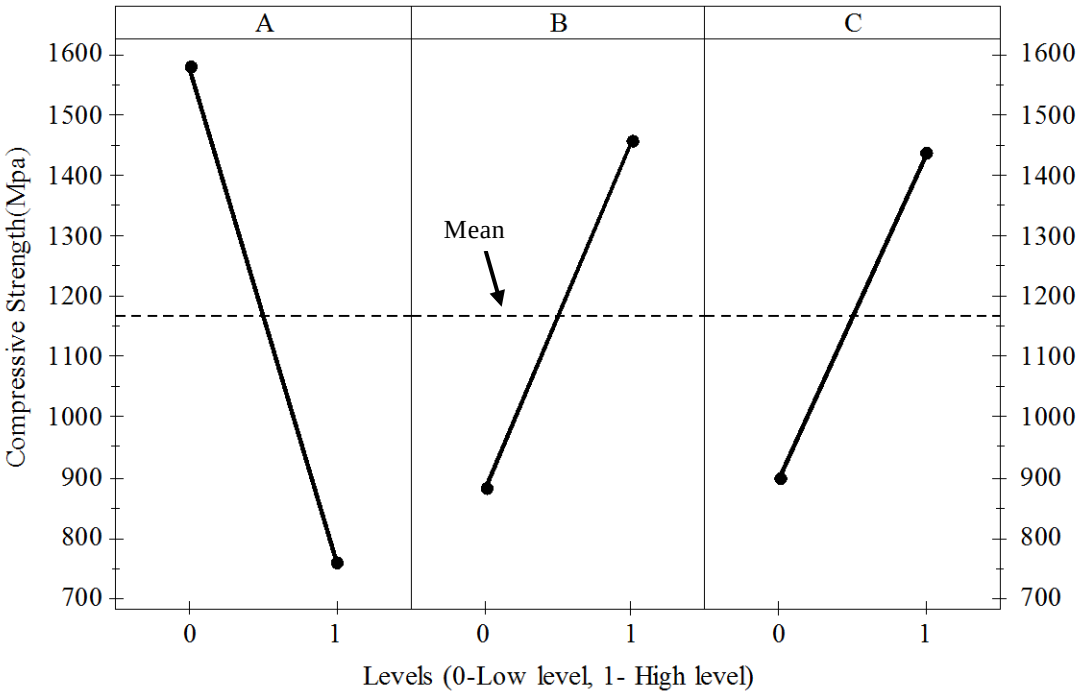


Figure 3.1-1: Main effects plot of process parameters on compressive strength, A-Layer thickness (low- 50 µm, high- 100 µm), B-Sintering time (low- 2hours, high- 4 hours), C-Sintering temperature (low- 1120 °C, high- 1180°C)

The interaction effect of different parameters on compressive strength is shown in Figure 3.1-2. From interaction plot, it is clear that the interaction between sintering time and sintering temperature has significant effect on compressive strength compared to layer thickness and sintering time interaction effect, layer thickness and sintering temperature interaction effect. Sintering time and sintering temperature interactive effect is highly significant on compressive strength of the fabricated sample. The interaction between layer thickness and sintering time, layer thickness and sintering temperature doesn't seem to have much effect on compressive strength.

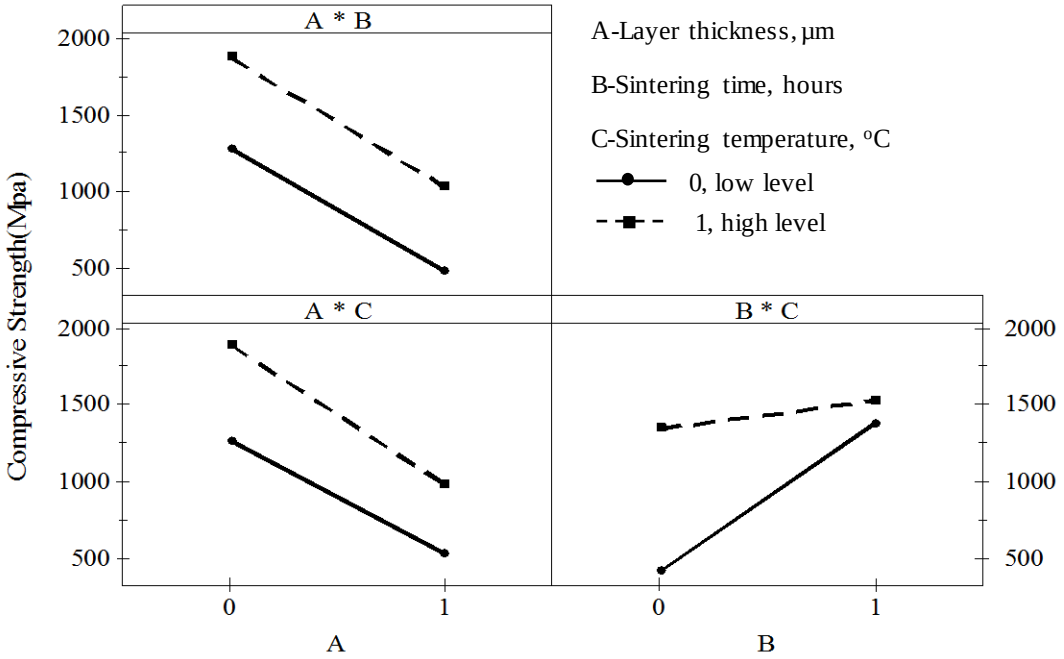


Figure 3.1-2: Interaction effects plot of process parameters on compressive strength, A*B refers interaction between Layer thickness and Sintering time, A*C refers interaction between Layer thickness and Sintering temperature, B*C refers interaction between Sintering temperature and Sintering time

The effect of different parameters on radial shrinkage rate is represented in Figure 3.1-3 and it reveals that three parameters are significant and radial shrinkage rate is low for sample fabricated with high layer thickness, shorter sintering time and lower sintering temperature It means higher layer thickness produced sample with low shrinkage rate than lower layer thickness, shorter sintering time produced sample with low shrinkage rate than longer sintering time, lower sintering temperature produced sample with low shrinkage rate than higher sintering temperature.

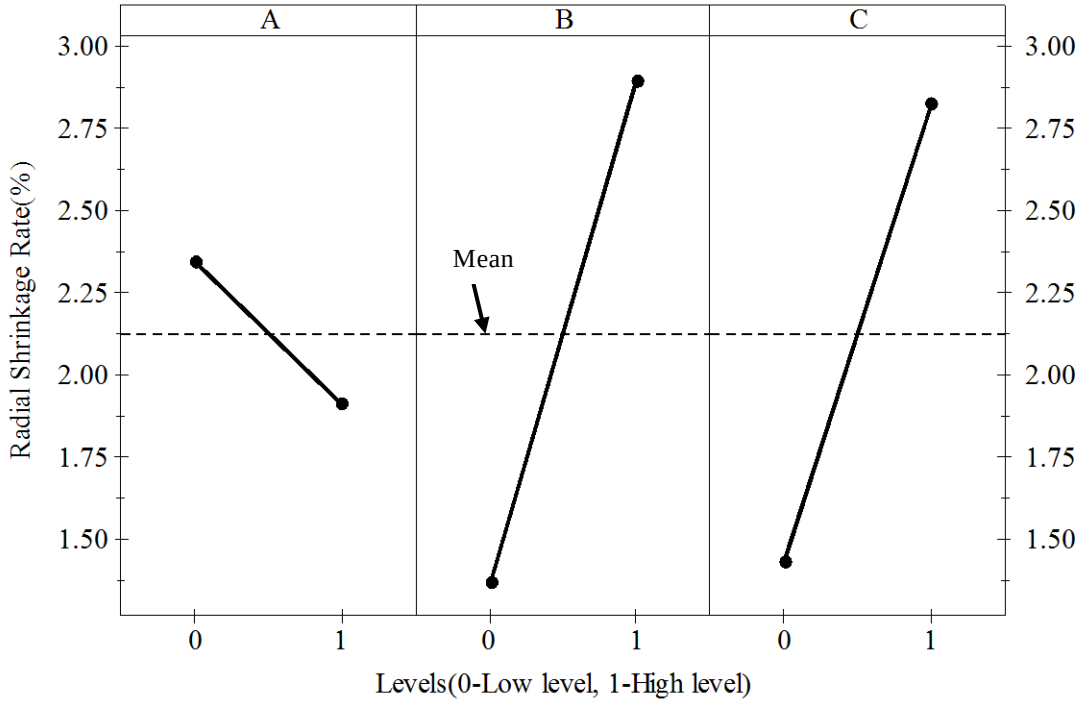


Figure 3.1-3: Main effects plot of process parameters on radial shrinkage rate, A-Layer thickness (low- 50 µm, high- 100 µm), B-Sintering time (low- 2hours, high- 4 hours), C-Sintering temperature (low- 1120 $^{o}$C, high- 1180$^{o}$C)

The interaction effect of different parameters on radial shrinkage is shown in Figure 3.1-4.From interactions plot, it is evident that the interaction between sintering time and sintering temperature has significant effect on radial shrinkage rate compared to layer thickness and sintering time interaction effect, layer thickness and sintering temperature interaction effect. Sintering time and sintering temperature interactive effect is highly significant on radial shrinkage of the fabricated sample. Similar to interaction effect plot of compressive strength, the interaction between layer thickness and sintering time, layer thickness and sintering temperature doesn't seem to have much effect on compressive strength.

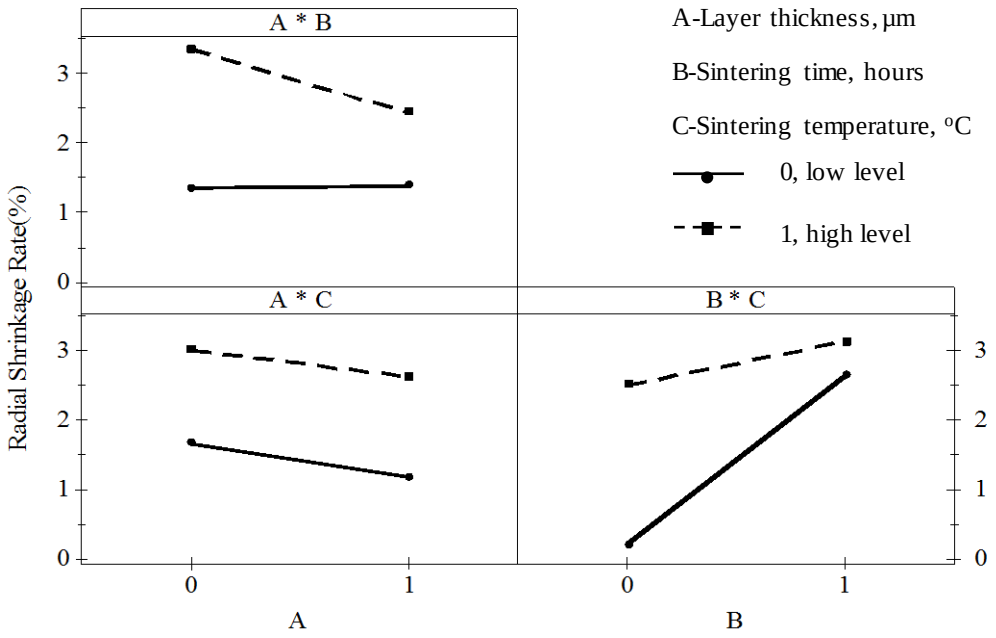


Figure 3.1-4: Interaction effects plot of process parameters on radial shrinkage rate, A*B refers interaction between Layer thickness and Sintering time, A*C refers interaction between Layer thickness and Sintering temperature, B*C refers interaction between Sintering temperature and Sintering time

Figure 3.1-5 shows the relationship between three factors layer thickness, sintering time and sintering temperature on longitudinal shrinkage rate. Main effects plot reveals that three parameters are significant and longitudinal shrinkage rate is low for sample fabricated with high layer thickness, shorter sintering time and lower sintering temperature. It means higher layer thickness produced sample with low shrinkage rate than lower layer thickness, shorter sintering time produced less shrinkage rate than longer sintering time, lower sintering temperature produced low shrinkage rate than higher sintering temperature. The main effects plot of longitudinal shrinkage is similar to that of radial shrinkage.

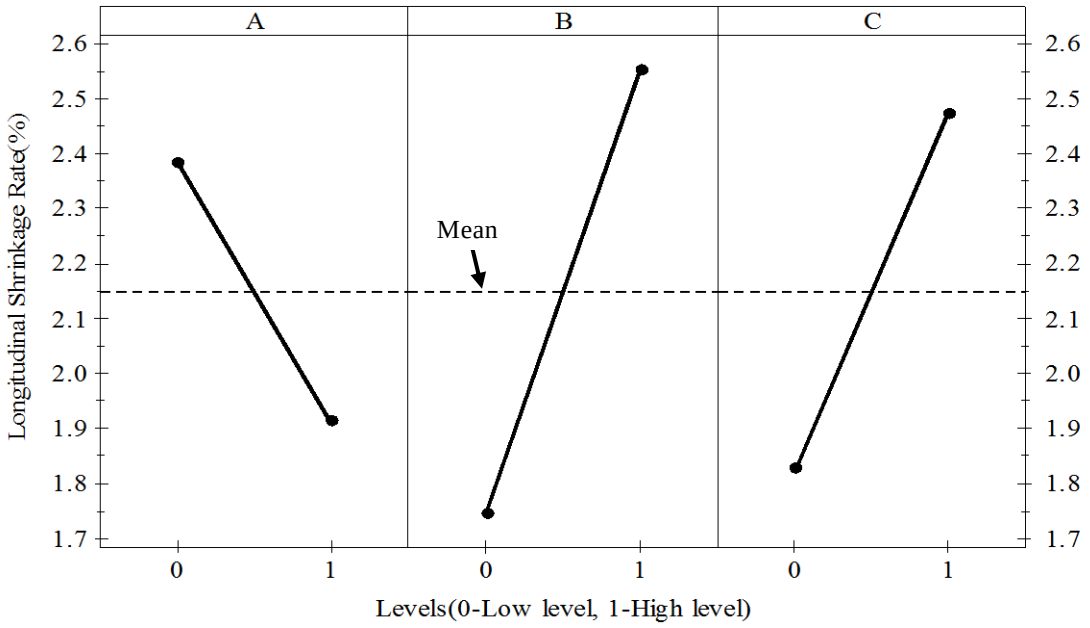


Figure 3.1-5: Main effects plot of process parameters on longitudinal shrinkage, A-Layer thickness (low- 50 µm, high- 100 µm), B-Sintering time (low- 2hours, high- 4 hours), C-Sintering temperature (low- 1120 °C, high- 1180°C)

Figure 3.1-6 reveals the combined influence of layer thickness and sintering time on longitudinal shrinkage rate. It is evident that the interaction between layer thickness and sintering time has significant effect on longitudinal shrinkage rate compared to sintering time and sintering temperature interaction effect, layer thickness and sintering temperature interaction effect.

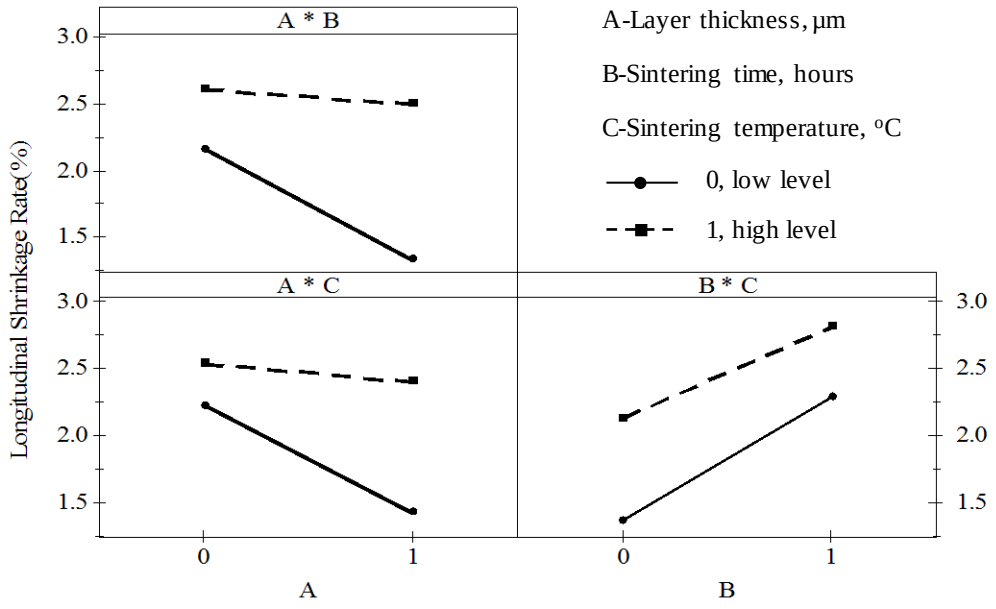


Figure 3.1-6: Interaction effects plot of process parameters on longitudinal shrinkage rate, A*B refers interaction between Layer thickness and Sintering time, A*C refers interaction between Layer thickness and Sintering temperature, B*C refers interaction between Sintering time and Sintering temperature

The main effects and interaction effects plots shows the impact of each factor whereas analysis of variance is performed to determine the significance of factors. The results of analysis give us the contribution percentage of each parameter namely, Layer thickness, Sintering time and temperature on Compressive Strength, Radial and Longitudinal shrinkage rate.

Table 3.1-2, 3.1-3, and 3.1-4 shows the analysis of variance results for compressive strength, longitudinal shrinkage and radial shrinkage rates.

Table 3.1-2: Results of Analysis of variance of compressive strength

| Factor | DF | SS | MS | F-Value |
|---|---|---|---|---|
| **A** | 1 | 2697166 | 2697166 | 123.82 |
| **B** | 1 | 1317456 | 1317456 | 60.48 |
| **C** | 1 | 1164899 | 1164899 | 53.48 |
| **A*B** | 1 | 2323 | 2323 | 0.11 |
| **A*C** | 1 | 31576 | 31576 | 1.45 |
| **B*C** | 1 | 612784 | 612784 | 28.13 |
| **A*B*C** | 1 | 8317 | 8317 | 0.38 |
| **Error** | 8 | 174265 | 21783 | |
| **Total** | 15 | 6008785 | | |

Table 3.1-3: Results of Analysis of variance of radial shrinkage rate

| Factor | DF | SS | MS | F-Value |
|---|---|---|---|---|
| **A** | 1 | 0.7455 | 0.74547 | 2.57 |
| **B** | 1 | 9.3547 | 9.35474 | 32.25 |
| **C** | 1 | 7.8086 | 7.80855 | 26.92 |
| **A*B** | 1 | 0.9305 | 0.93050 | 3.21 |
| **A*C** | 1 | 0.0103 | 0.01031 | 0.04 |
| **B*C** | 1 | 3.2377 | 3.23767 | 11.16 |
| **A*B*C** | 1 | 0.3643 | 0.36431 | 1.26 |
| **Error** | 8 | 2.3209 | 0.29011 | |
| **Total** | 15 | 24.7724 | | |

Table 3.1-4: Results of Analysis of variance of longitudinal shrinkage rate

| Factor | DF | SS | MS | F-Value |
|---|---|---|---|---|
| **A** | 1 | 0.88831 | 0.88831 | 2.42 |
| **B** | 1 | 2.60016 | 2.60016 | 7.08 |
| **C** | 1 | 1.67056 | 1.67056 | 4.55 |
| **A*B** | 1 | 0.51481 | 0.51481 | 1.40 |
| **A*C** | 1 | 0.44556 | 0.44556 | 1.21 |
| **B*C** | 1 | 0.05641 | 0.05641 | 0.15 |
| **A*B*C** | 1 | 0.00601 | 0.00601 | 0.02 |
| **Error** | 8 | 2.93605 | 0.36701 | |
| **Total** | 15 | 9.11784 | | |

Percentage Contribution factor, PC= SS of factor/ Total (SS of each factor). Example: Contribution of A on compressive strength is calculated by SS (A)/SS (A+B+C), from the Table 3.1-1, % contribution of A on compressive strength is 52%.

Figure 3.1-7a shows that layer thickness has high significance of 52% on compressive strength among all the three parameters. From Figure 3.1-7b and 3.17c, it is evident that sintering time has significant effect of 52% and 51% on radial and longitudinal shrinkage rates. Parameters need to be optimized to obtain desired output with less quality variation, the printed sample should be dimensionally accurate which is critical in many engineering applications like biomedical, aerospace, automobile industries.

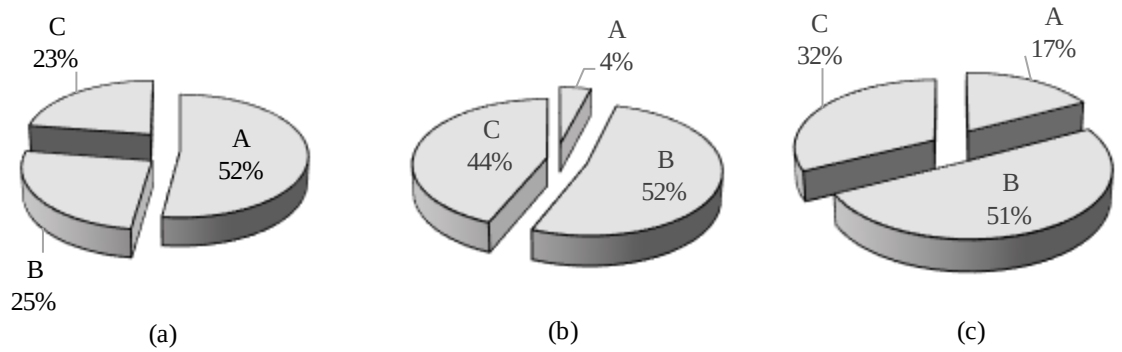


Figure 3.1-7: Percentage contributions on (a) Compressive Strength (b) Radial shrinkage rate (c) Longitudinal shrinkage rate. A-Layer thickness, B-Sintering time and C-Sintering temperature

### 3.1.2 Circular Lattice Structure

The main effects and interaction effects plot of build parameters on compressive strength and shrinkage rates of circular structure reveals similar results as of solid structure. The compressive strength, radial and longitudinal shrinkage for circular samples made with different experimental settings were calculated and presented in Table 3.1-5.

Table 3.1-5: Experimental results, where A: Layer Thickness, B: Sintering time and C: Sintering temperature

| # | A | B | C | Compressive Strength(Mpa) | Radial Shrinkage (%) | Longitudinal Shrinkage (%) |
|---|---|---|---|---|---|---|
| 1 | 0 | 0 | 0 | 160.3 | 1.7 | 1.3 |
| 2 | 0 | 0 | 1 | 654.3 | 2.5 | 3.6 |
| 3 | 0 | 1 | 0 | 739.9 | 4.0 | 3.7 |
| 4 | 0 | 1 | 1 | 998.6 | 5.8 | 3.9 |
| 5 | 1 | 0 | 0 | 12.8 | 0 | 0.1 |
| 6 | 1 | 0 | 1 | 303.3 | 1.5 | 3.3 |
| 7 | 1 | 1 | 0 | 229.33 | 1.6 | 3.0 |
| 8 | 1 | 1 | 1 | 545.5 | 3.6 | 4.1 |

It seems that layer thickness is the most significant factor on compressive strength, sintering time being the most significant parameter on shrinkage rates. The interaction of sintering parameters is high compared to other interactions on mechanical properties of circular structure. Table 3.1-6, 3.1-7, and 3.1-8 shows the analysis of variance results for compressive strength, longitudinal shrinkage and radial shrinkage rates of circular structure and Figure 3.1-8 represents significance of each parameter.

Table 3.1-6: Results of Analysis of variance for compressive strength

| Factor | DF | SS | MS | F-Value |
|---|---|---|---|---|
| **A** | 1 | 658670 | 658670 | 730.8 |
| **B** | 1 | 373095 | 373095 | 413.95 |
| **C** | 1 | 359023 | 359023 | 398.34 |
| **A*B** | 1 | 23130 | 23130 | 25.66 |
| **A*C** | 1 | 56 | 56 | 0.06 |
| **B*C** | 1 | 591 | 591 | 0.66 |
| **A*B*C** | 1 | 2499 | 2499 | 2.77 |
| **Error** | 8 | 7210 | 901 | |
| **Total** | 15 | 1424274 | | |

Table 3.1-7: Results of Analysis of variance for radial shrinkage rate

| Factor | DF | SS | MS | F-Value |
|---|---|---|---|---|
| **A** | 1 | 13.9689 | 13.9689 | 6.26 |
| **B** | 1 | 21.7389 | 21.7389 | 9.74 |
| **C** | 1 | 9.1658 | 9.1658 | 4.11 |
| **A*B** | 1 | 0.8696 | 0.8696 | 0.39 |
| **A*C** | 1 | 0.2426 | 0.2426 | 0.11 |
| **B*C** | 1 | 0.5663 | 0.5663 | 0.25 |
| **A*B*C** | 1 | 0.0743 | 0.0743 | 0.03 |
| **Error** | 8 | 17.8489 | 2.2311 | |
| **Total** | 15 | 64.4751 | | |

Table 3.1-8: Results of Analysis of variance for longitudinal shrinkage rate

| Factor | DF | SS | MS | F-Value |
|---|---|---|---|---|
| **A** | 1 | 0.8953 | 0.8953 | 0.91 |
| **B** | 1 | 10.4084 | 10.4084 | 10.63 |
| **C** | 1 | 10.931 | 10.931 | 11.17 |
| **A*B** | 1 | 0.2665 | 0.2665 | 0.27 |
| **A*C** | 1 | 0.8394 | 0.8394 | 0.86 |
| **B*C** | 1 | 4.3106 | 4.3106 | 4.4 |
| **A*B*C** | 1 | 0.0029 | 0.0029 | 0 |
| **Error** | 8 | 7.8311 | 0.9789 | |
| **Total** | 15 | 35.4851 | | |

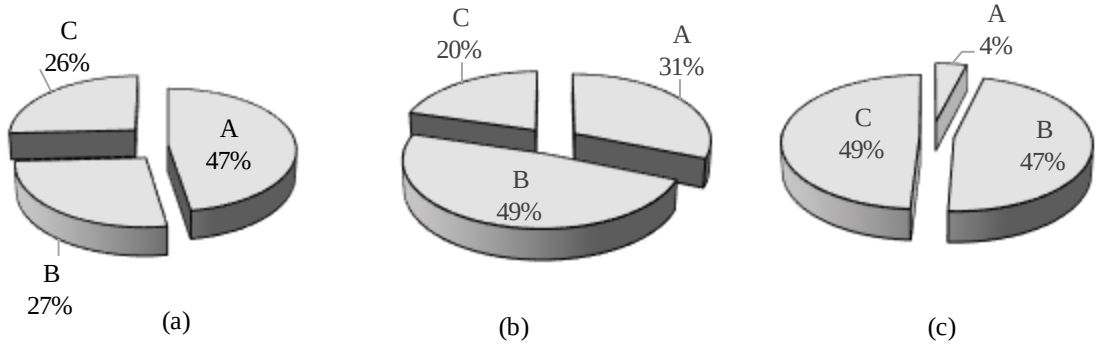


Figure 3.1-8: Percentage contributions on (a) Compressive Strength (b) Radial shrinkage rate (c) Longitudinal shrinkage rate. A-Layer thickness, B-Sintering time and C-Sintering temperature

### 3.1.3 Cubical Lattice Structure

The compressive strength, radial and longitudinal shrinkage for cubical samples made with different experimental settings were calculated and presented in Table 3.1-9.

Table 3.1-9: Experimental results, where A: Layer Thickness, B: Sintering time and C: Sintering temperature

| # | A | B | C | Compressive Strength(Mpa) | Radial Shrinkage (%) | Longitudinal Shrinkage (%) |
|---|---|---|---|---|---|---|
| 1 | 0 | 0 | 0 | 154.5 | 0.43 | 1.2 |
| 2 | 0 | 0 | 1 | 545.2 | 5.2 | 3.5 |
| 3 | 0 | 1 | 0 | 612.3 | 4.6 | 3.2 |
| 4 | 0 | 1 | 1 | 958.3 | 5.25 | 4.1 |
| 5 | 1 | 0 | 0 | 11.6 | 0 | 0.1 |
| 6 | 1 | 0 | 1 | 250.9 | 4.2 | 3.5 |
| 7 | 1 | 1 | 0 | 253.2 | 3.7 | 3.1 |
| 8 | 1 | 1 | 1 | 326.4 | 4.8 | 3.8 |

The main effects and interaction effects plot of build parameters on compressive strength and shrinkage rates of circular structure reveals that the compressive strength is highly influenced by layer thickness, sintering temperature being the most significant parameter on shrinkage rates. The interaction of sintering parameters is high compared to other interactions on mechanical properties of circular structure. Table 3.1-10, 3.1-11, and 3.1-12 shows the analysis of variance results for compressive strength, longitudinal shrinkage and radial shrinkage rates of circular structure and Figure 3.1-9 represents significance of each parameter.

Table 3.1-10: Results of Analysis of variance for compressive strength

| Factor | DF | SS | MS | F-Value |
|---|---|---|---|---|
| **A** | 1 | 509939 | 509939 | 1943.83 |
| **B** | 1 | 352836 | 352836 | 1344.97 |
| **C** | 1 | 275205 | 275205 | 1049.05 |
| **A*B** | 1 | 76674 | 76674 | 292.27 |
| **A*C** | 1 | 44986 | 44986 | 171.48 |
| **B*C** | 1 | 11109 | 11109 | 42.35 |
| **A*B*C** | 1 | 3684 | 3684 | 14.04 |
| **Error** | 8 | 2099 | 262 | |
| **Total** | 15 | 1276532 | | |

Table 3.1-11: Results of Analysis of variance for radial shrinkage rate

| Factor | DF | SS | MS | F-Value |
|---|---|---|---|---|
| **A** | 1 | 1.7556 | 1.7556 | 22.25 |
| **B** | 1 | 18.5761 | 18.5761 | 235.48 |
| **C** | 1 | 28.5156 | 28.5156 | 361.47 |
| **A*B** | 1 | 0.0081 | 0.0081 | 0.1 |
| **A*C** | 1 | 0.0064 | 0.0064 | 0.08 |
| **B*C** | 1 | 13.286 | 13.286 | 168.42 |
| **A*B*C** | 1 | 0.2256 | 0.2256 | 2.86 |
| **Error** | 8 | 0.6311 | 0.0789 | |
| **Total** | 15 | 63.0046 | | |

Table 3.1-12: Results of Analysis of variance for longitudinal shrinkage rate

| Factor | DF | SS | MS | F-Value |
|---|---|---|---|---|
| **A** | 1 | 0.4692 | 0.4692 | 1.51 |
| **B** | 1 | 8.5849 | 8.5849 | 27.6 |
| **C** | 1 | 13.7641 | 13.7641 | 44.25 |
| **A*B** | 1 | 0.1521 | 0.1521 | 0.49 |
| **A*C** | 1 | 0.1681 | 0.1681 | 0.54 |
| **B*C** | 1 | 4.3056 | 4.3056 | 13.84 |
| **A*B*C** | 1 | 0.3782 | 0.3782 | 1.22 |
| **Error** | 8 | 2.4887 | 0.3111 | |
| **Total** | 15 | 30.311 | | |

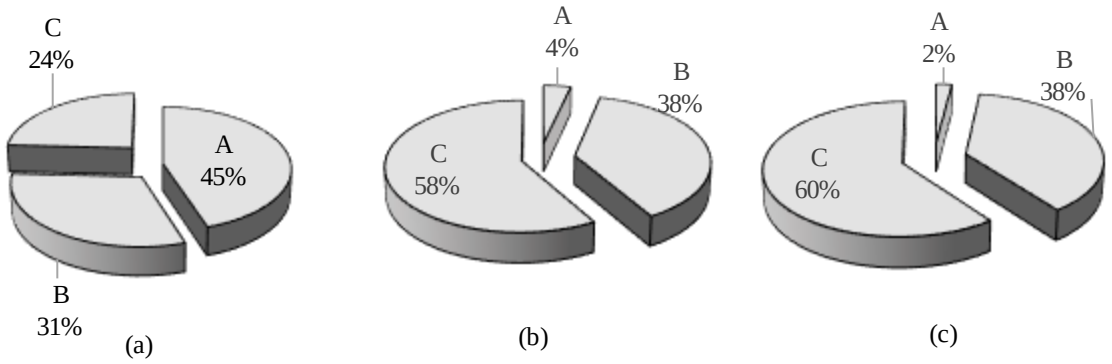


Figure 3.1-9: Percentage contributions on (a) Compressive Strength (b) Radial shrinkage rate (c) Longitudinal shrinkage rate. A-Layer thickness, B-Sintering time and C-Sintering temperature

The process parameters layer thickness, sintering time and sintering temperature are optimized based on the above analysis for maximum compressive strength, minimum shrinkage in radial and longitudinal directions. Also, parameter optimization is done for combined properties of high compressive strength with low shrinkage rates, represented in Table 3.1-13. The optimal parameters for high compressive strength are 50µm layer thickness, 4 hours sintering time and 1180 $^{o}$C sintering temperature and for low shrinkage rates are 100µm layer thickness, 2 hours sintering time and 1120 $^{o}$C sintering temperature. The parameters for optimized response is listed in the below Table 3.1-13.

Table 3.1-13: Optimized parameters

| **S. No** | **Optimized Response** | **A-Layer thickness, µm** | **B-Sintering time, hours** | **C-Sintering temperature, $^{o}$C** |
|---|---|---|---|---|
| **1** | High Compressive Strength | 50 | 4 | 1180 |
| **2** | Radial shrinkage rate | 100 | 2 | 1120 |
| **3** | Longitudinal shrinkage rate | 100 | 2 | 1120 |
| **4** | High Compressive Strength with low Shrinkage Rates | 50 | 2 | 1120 |

### 3.1.4 Discussion

The study of effect of build parameters namely layer thickness, sintering time and sintering temperature on compressive strength, shrinkage rates reveals the following information. Lower layer thickness has high compressive strength compared to that of higher layer thickness. Sintering parameters has significant effect on shrinkage in radial and longitudinal directions. Interaction between sintering time and sintering temperature has strongest influence on compressive strength, radial, and longitudinal shrinkage rates. The sample fabricated in experimental setup with longest sintering time and highest sintering temperature has high compressive strength, high radial, and longitudinal shrinkage values. The possible reasons for above conclusions are discussed below.

The reason for sample fabricated with lower layer thickness having more compressive strength compared to that of high layer thickness is that lower the layer thickness higher is the number of layers in printing. With higher number of layers, the integrity would be higher leading to high mechanical strengths. With binder saturation being same in the study, binder would penetrate more if layer thickness is less hence producing stable samples. Under same binder saturation setting, strong bond will take place if the layer thickness is low, shown in Figure 3.1-10a whereas binder is not enough to strongly bond the powder materials together as shown in Figure 3.1-10b.

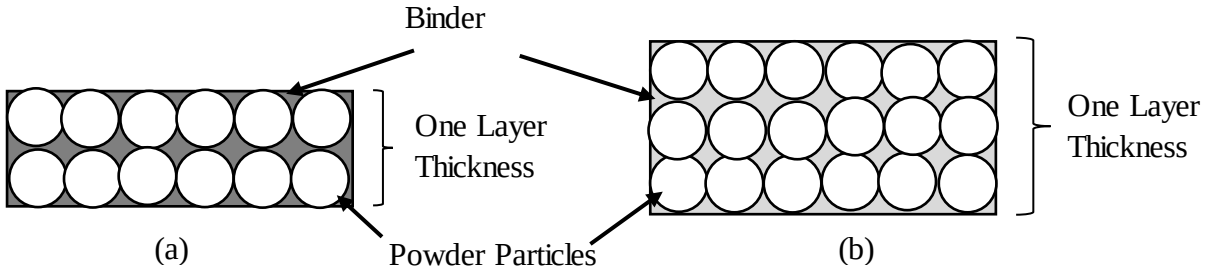


Figure 3.1-10:(a) Lower layer thickness showing better binder distribution, (b) Higher layer thickness showing poor binder distribution

Sintering time and Sintering temperature has the most significant effect on radial and longitudinal directions due to the matter of fact that the loose powders sinter together causing the sample to shrink and results in lesser pores. There are two types of mass transportation during the sintering, surface and bulk transport. Necking happens during the surface transportation and bulk transport is the main contributor to mass flow through diffusion. The process of sintering has three stages: initial, intermediate and final stage [62]. In the initial stage, the particles come in to contact as shown in Figure 3.1-11a and the green part has low physical integrity because of less bond between the particles. In the intermediate state, bonding takes place between the adjacent powder particles forming the neck, the pore structure becomes smooth and develops an interconnection as shown in Figure 3.1-11b. In the final stage, pores are closed making a compact solid.

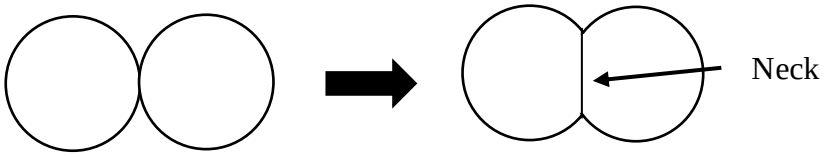


Figure 3.1-11: (a) Adhesion between powder particles (b) Growth of interparticle neck

Sintering is a diffusion controlled mechanism where reduction of free space operates as driving force, the solid mass is created by atoms diffusing across the particle boundaries. With the increase in sintering time and sintering temperature, particles connected closer thus the structure became more compact and strong providing higher compressive strength. Compressive strength observed to be increased with increase in values of sintering parameters. Scanning Electron Microscope (SEM) JEOL JSM-6510MV was used to study the samples at micro level. SEM analysis shown in Figure 3.1-12-Figure 3.1-15, demonstrates the strong influence of sintering time and sintering temperature on the grain size and morphology. The neck to diameter (X/D) shown

in Figure 3.1-13, is calculated for sample fabricated in each experiment using SEM images and it is found that neck to diameter ratios are for 0.21, 0.33, 0.38 and 0.44.

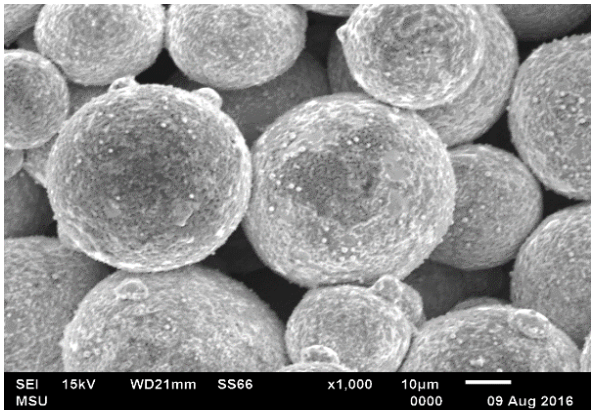


Figure 3.1-12: SEM image of sample made at Sintering time: 2 hours, temperature: 1120 °C

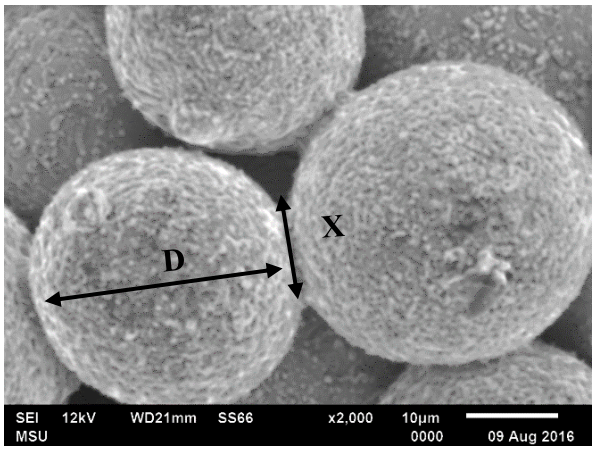


Figure 3.1-13: SEM image of sample made at Sintering time: 2 hours, temperature: 1180 °C

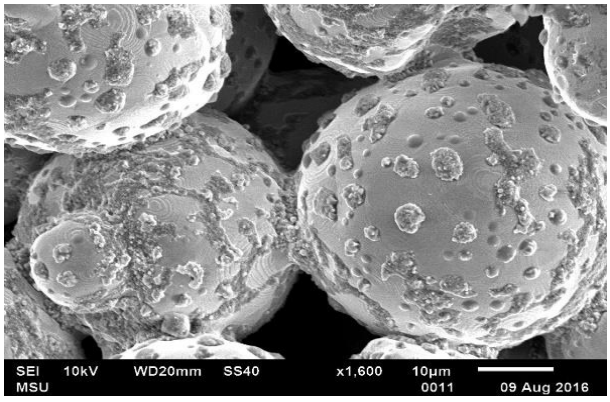


Figure 3.1-14: SEM image of sample made at Sintering time: 4 hours, temperature: 1120 °C

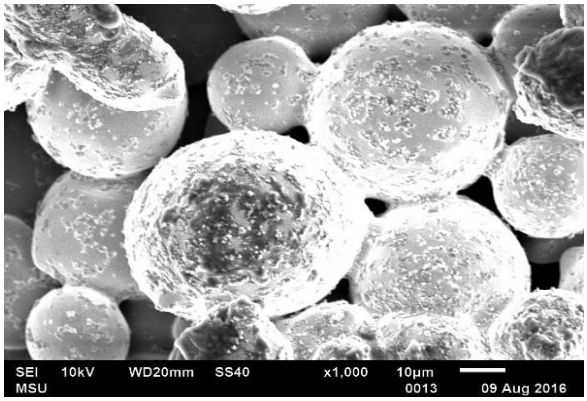


Figure 3.1-15: SEM image of sample made at Sintering time: 4 hours, temperature: 1180 $^{o}$C

The necking is high for experiment with long sintering time and sintering temperature and it is understandable that compressive strength is maximum for sample with high sintering time and sintering temperature because of strong bonding between the particles at micro level. Therefore, controlling sintering time and sintering temperature at lower layer thickness will produce a sample with high compressive strengths and less shrinkage rates.

## 3.2 NEURAL NETWORK RESULTS

1. First case: The data used for testing is from compression testing of solid structure.
2. Second case: The data used for testing is from compression testing of circular structure.
3. Third case: The data used for testing from compression testing of cubical structure.

### 3.2.1 Solid Structure

With the normalized data in Table 3.2-1, the feedforward backpropagation network was trained with seven datasets leaving behind the one data set of experiment 7 for testing the network performance.

Table 3.2-1: Inputs A (Layer thickness), B (Sintering time), C (Sintering temperature) along with normalized output of compressive strength in the range of 0 to 1.

| # | A (Layer thickness) | B (Sintering time) | C (Sintering temperature) | Y (Compressive Strength, Mpa) | Output(O) |
|---|---|---|---|---|---|
| **1** | 0 | 0 | 0 | 745.5 | 0.350752 |
| **2** | 0 | 0 | 1 | 1780.5 | 0.89863 |
| **3** | 0 | 1 | 0 | 1811 | 0.914775 |
| **4** | 0 | 1 | 1 | 1972 | 1 |
| **5** | 1 | 0 | 0 | 82.89 | 0 |
| **6** | 1 | 0 | 1 | 879.5 | 0.421685 |
| **7** | 1 | 1 | 0 | 978.5 | 0.474091 |
| **8** | 1 | 1 | 1 | 1083.5 | 0.529673 |
| Maximum value in Y column | | | | 1972 | |
| Minimum value in Y column | | | | 82.89 | |

The error graph for model during the training is plotted using the error value obtained in each iteration, as shown in Figure 3.2-1, where it can be seen that necessary iterations to reach the goal was approximately 7500 iterations, high iterations signifies the acuteness of carried calculations. From 15 to 7500 iterations, the error was changing in decimal places hence the straight line. The method is developed such that the neural network stops training once the error between network output and actual output is less than absolute value of 0.05.

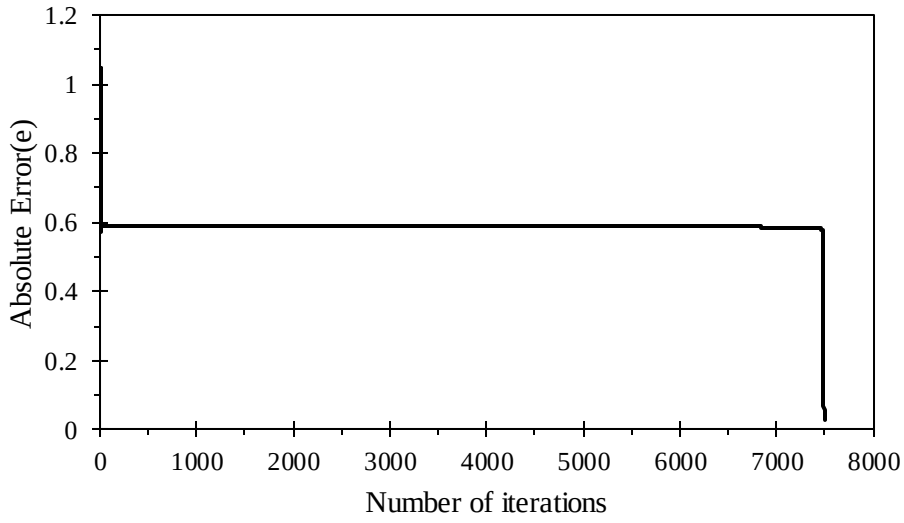


Figure 3.2-1: Training error vs number of iterations for the neural network model

Different learning rates were presented to network from 0.1 to 2 and the training error is plotted against learning rate as shown in the Figure 3.2-2. The maximum error in training allowed was 0.05 absolute value. The optimum learning rate for minimum error was found to be 0.6 in the training phase for the network. The network is tested for a target value of 0.47 and the value obtained from the network is 0.4884.

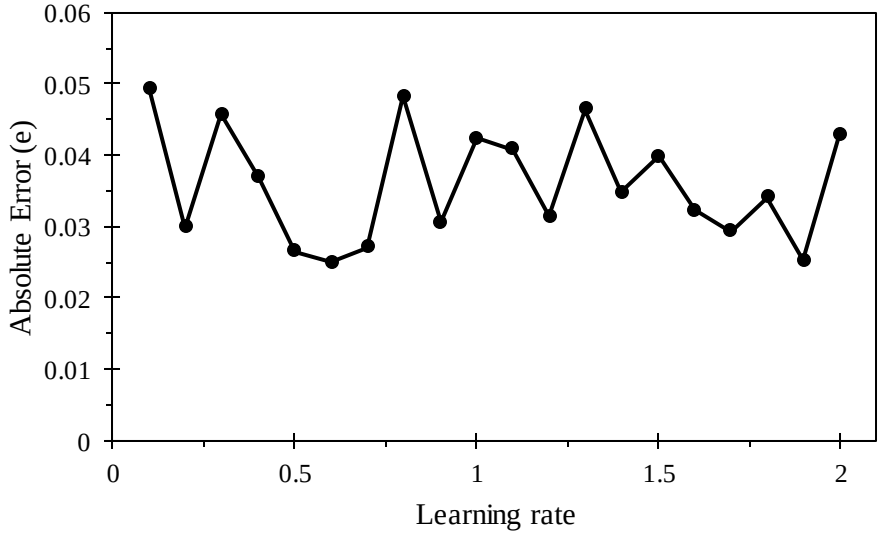


Figure 3.2-2: Performance of network architecture for different learning rates

### 3.2.2 Circular Lattice Structure

The same feed forward back propagation network used for predicting the compressive strength of solid is used for training and testing the compressive strength of circular and cubical lattice structure. The compressive strength of samples fabricated using eight experimental settings are normalized along with inputs, shown in the Table 3.2-2. Data obtained from experiment 2 is used for testing the network while remaining data is used to train the network.

Table 3.2-2: Normalized inputs and output values of circular structure

| # | A (Layer thickness) | B (Sintering time) | C (Sintering temperature) | Y (Compressive Strength, Mpa) | Output(O) |
|---|---|---|---|---|---|
| **1** | 0 | 0 | 0 | 160.3 | 0.14 |
| **2** | 0 | 0 | 1 | 654.3 | 0.65 |
| **3** | 0 | 1 | 0 | 739.9 | 0.73 |
| **4** | 0 | 1 | 1 | 998.6 | 1 |
| **5** | 1 | 0 | 0 | 12.8 | 0 |
| **6** | 1 | 0 | 1 | 303.3 | 0.29 |
| **7** | 1 | 1 | 0 | 229.33 | 0.21 |
| **8** | 1 | 1 | 1 | 545.5 | 0.54 |
| Maximum value in Y column | | | | 998.6 | |
| Minimum value in Y column | | | | 12.8 | |

The error graph for neural network model during the training is plotted using the error value obtained in each iteration, as shown in Figure 3.2-3, where it can be seen that necessary iterations to reach the goal was approximately 200000 iterations. From 100 to 199000 iterations, the error was changing in decimal places hence the straight line.

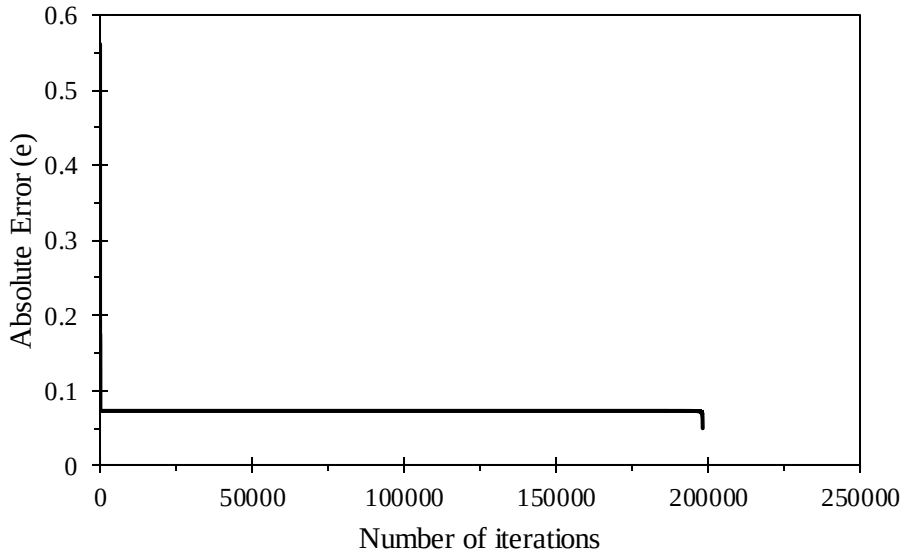


Figure 3.2-3: Training error vs number of iterations for the neural network model

Different learning rates were presented to network from 0.1 to 2 and the training error is plotted against learning rate as shown in the Figure 3.2-4. The maximum error in training allowed was 0.05 absolute value. The optimum learning rate for minimum error was found to be 2 in the training phase for the network. The network is tested for a target value of 0.65 and the value obtained from the network is 0.6784.

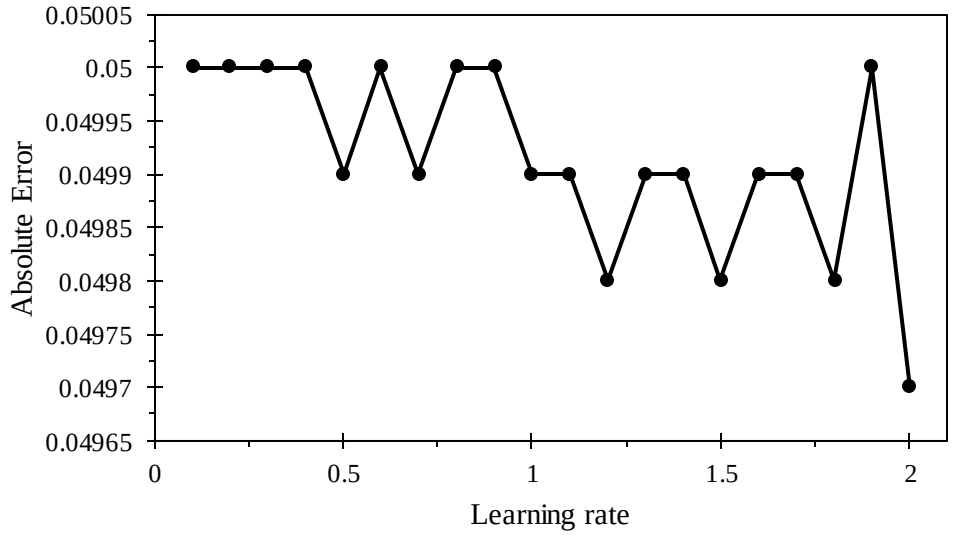


Figure 3.2-4: Performance of network architecture for different learning rates

### 3.2.3 Cubical Lattice Structure

The compressive strength of cubical samples fabricated using eight experimental settings are normalized along with inputs, shown in the Table 3.2-3. Data obtained from experiment 6 is used for testing the network while remaining data is used to train the network.

Table 3.2-3: Normalized inputs and output values of cubical structure

| # | A (Layer thickness) | B (Sintering time) | C (Sintering temperature) | Y (Compressive Strength, Mpa) | Output(O) |
|---|---|---|---|---|---|
| **1** | 0 | 0 | 0 | 154.5 | 0.15 |
| **2** | 0 | 0 | 1 | 545.2 | 0.56 |
| **3** | 0 | 1 | 0 | 612.3 | 0.63 |
| **4** | 0 | 1 | 1 | 958.3 | 1 |
| **5** | 1 | 0 | 0 | 11.6 | 0 |
| **6** | 1 | 0 | 1 | 250.9 | 0.25 |
| **7** | 1 | 1 | 0 | 253.2 | 0.26 |
| **8** | 1 | 1 | 1 | 326.4 | 0.33 |
| Maximum value in Y column | | | | 958.3 | |
| Minimum value in Y column | | | | 11.6 | |

The error graph for neural network model during the training is plotted using the error value obtained in each iteration, as shown in Figure 3.2-5, where it can be seen that necessary iterations to reach the goal was approximately 7500 iterations. From 75 to 7500 iterations, the error was changing in decimal places hence the straight line.

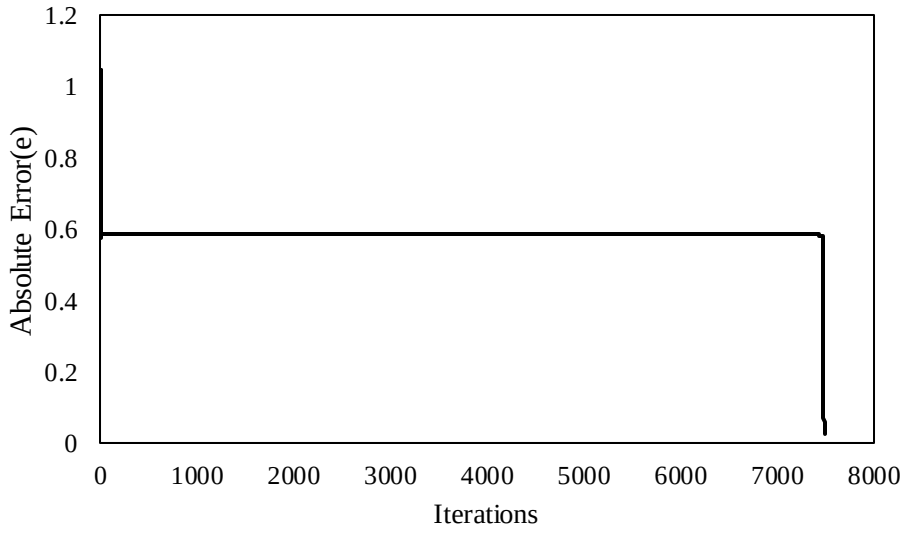


Figure 3.2-5: Training error vs number of iterations for the neural network model

Different learning rates were presented to network from 0.1 to 2 and the training error is plotted against learning rate as shown in the Figure 3.2-6. The maximum error in training allowed was 0.05 absolute value. The optimum learning rate for minimum error was found to be 2 in the training phase for the network. The network is tested for a target value of 0.25 and the value obtained from the network is 0.2759.

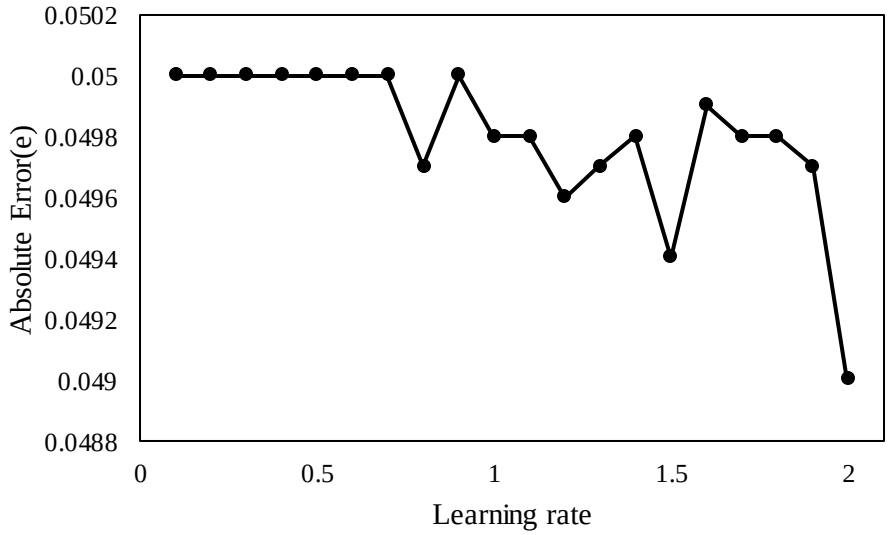


Figure 3.2-6: Performance of network architecture for different learning rates

The data obtained for the above cases using neural network is denormalized and the values are tabulated below. Table 3.2-4 represents the actual compressive strength value for different structures obtained using experimentation and the value obtained using neural network.

Table 3.2-4: Neural network results for different structures

| Structure | Actual Compressive Strength (Mpa) | Predicted Compressive Strength (Mpa) | Difference (%) |
|---|---|---|---|
| **Solid** | 978.5 | 1005.5 | 2.75 |
| **Circular** | 654.3 | 681.5 | 4.15 |
| **Cubical** | 250.9 | 273.9 | 9.16 |

The prediction values were found to be in good agreement with that of experimental values, the maximum difference being 9.16%. The values obtained using neural network are slightly greater than actual values obtained using experimentation. The prediction performance can be improved further either by changing the number of hidden nodes used in the study or by using a different architecture. It should also be noted that the performance of network or the difference % reduces and the network becomes robust as it is presented with more sets of data, the current study has only eight sets of data. The difference will be more consistent and the target value will be close to predicted as the network gets more sets of data for training. The current model is validated using the work found in literature and the validation of current neural network model using data from literature is presented in next section. The neural network uses backpropagation algorithm as training algorithm, sigmoid function as activation function and network has one hidden layer. The current model helps to identify the input parameters set up for desired output without experimentation and it serves as a tool to predict the compressive strength of sample over the range of layer thickness, sintering time and sintering temperature. The advantage of this approach is that it can be used for any material and can be trained for any desired output given the experimental data.

The study indicates the ability of feed forward back propagation neural network as a good technique for determining the compressive strength of binder jetting samples and reveals the applications on neural network in material science and engineering particularly in complex fields like additive manufacturing as it involves many physical phenomena.

The current model can be used to develop feedforward artificial neural network using backpropagation training algorithm if the user wants to use the same features. However, depending on the input parameters, output parameters, number of hidden layers, activation function the code has to be modified accordingly. Figure 3.2-7 shows the methodology to develop the neural network model provided the data for testing and training.

First step is to normalize the input values and output values from the experimental data. Data normalization prior to training process is crucial to obtain good results as well as to fasten significantly the calculations [63]. Based on the number of input and output parameters decide on the architecture of feedforward neural network, the number of hidden layers and hidden nodes in the structure. The network architecture has significant effect on prediction results. However, the optimal number of hidden layers, optimal number of hidden nodes depend on specific problem to be handled and there is no straightforward method to determine them [64]. Once the architecture is decided, training algorithm and activation function has to be chosen, the current study used back propagation algorithm with sigmoid activation function. With the normalized input values, target values, network architecture, activation function the model can be developed according to the training algorithm.

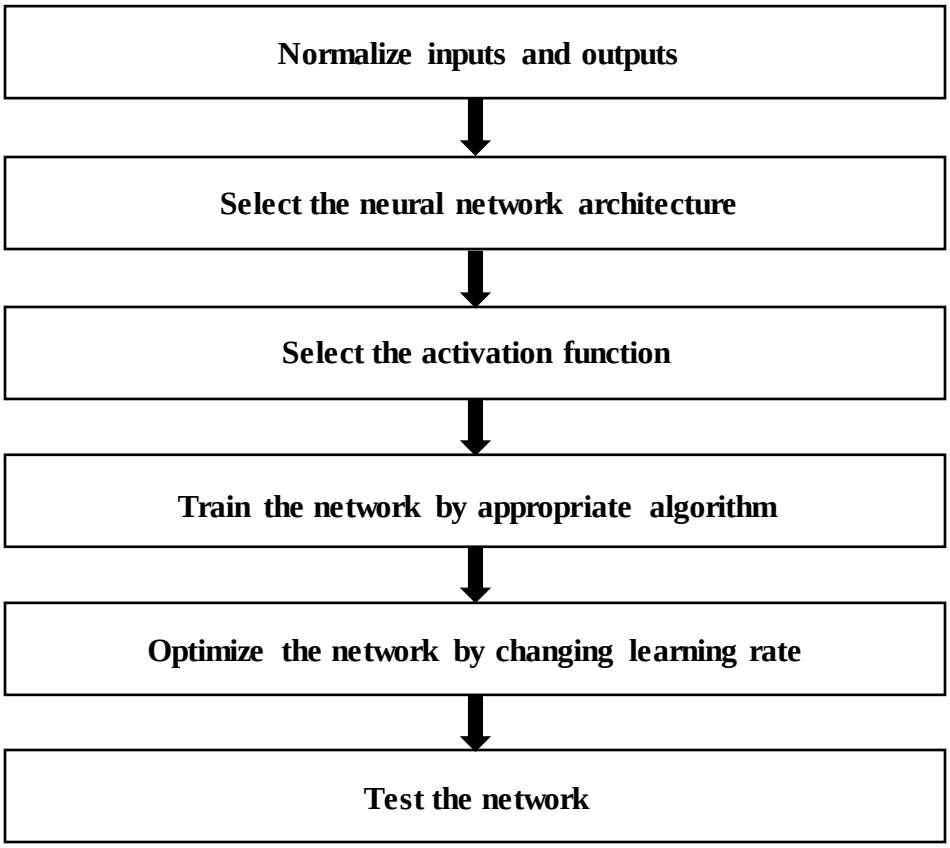


Figure 3.2-7: Methodology to develop own model

### 3.2.4 Model Validation

The current model was used for predicting the values from the work found in literature and the results are presented below. The study used neural network model to predict the hardness of shielded metal arc welded joints given the input of current, voltage, welding speed, magnetic field [65]. The data is obtained from literature and tabulated as shown in Table 3.2-5. First 18 experiments were used for training and the remaining experiments for testing. The difference between the actual hardness and predicted hardness using the current model is also represented in Table 3.2-6.

Table 3.2-5: Data from experimentation found in literature

| Exp # | Current(A) | Voltage(V) | Welding speed(mm/min) | Magnetic field(Gauss) | Hardness |
|---|---|---|---|---|---|
| 1 | 90 | 24 | 40 | 0 | 90 |
| 2 | 90 | 24 | 40 | 20 | 90 |
| 3 | 90 | 24 | 40 | 40 | 90 |
| 4 | 90 | 24 | 40 | 60 | 92 |
| 5 | 90 | 24 | 40 | 80 | 94 |
| 6 | 95 | 20 | 60 | 60 | 91 |
| 7 | 95 | 21 | 60 | 60 | 88 |
| 8 | 95 | 22 | 60 | 60 | 86 |
| 9 | 95 | 23 | 60 | 60 | 84 |
| 10 | 95 | 24 | 60 | 60 | 82 |
| 11 | 100 | 22 | 40 | 40 | 88 |
| 12 | 100 | 22 | 60 | 40 | 90 |
| 13 | 100 | 22 | 80 | 40 | 93 |
| 14 | 90 | 20 | 80 | 20 | 89 |
| 15 | 95 | 20 | 80 | 20 | 86 |
| 16 | 100 | 20 | 80 | 20 | 84 |
| 17 | 105 | 20 | 80 | 20 | 83 |
| 18 | 110 | 20 | 80 | 20 | 80 |

Table 3.2-6: Validation of neural network model

| Exp # | Actual Value of Hardness | Prediction value from Literature | Prediction value using current model | Difference % |
|---|---|---|---|---|
| 19 | 91 | 85.6 | 90.96 | 0.04 |
| 20 | 86 | 85.1 | 93.7 | 8.9 |
| 21 | 89 | 85.4 | 93.84 | 5.4 |
| 22 | 89 | 85.2 | 87.6 | 1.54 |
| 23 | 81 | 84.8 | 82.64 | 2.02 |
| 24 | 78 | 84.6 | 82.8 | 6.1 |
| 25 | 79 | 83.9 | 81.04 | 2.58 |

The maximum difference between the actual value and value predicted using current model is 8.9 % and the maximum difference found in literature is 8.46%. The small difference in prediction value from literature and prediction value using current model is because the model used in

literature has different architecture compared to the current model. Therefore, the current model seems to be in good agreement with the results found from the literature.

## 3.3 FINITE ELEMENT ANALYSIS

Compressive behavior of different lattice configurations was simulated using finite element software ANSYS. Multilinear isotropic hardening plasticity model is used to capture the nonlinear behavior of material. The ultimate compressive strength of material was determined from the experimental compression testing of binder jetting made solid cylindrical sample. A Poisson's ratio of 0.3 was assumed. Material properties listed in Table 3.3-1 along with stress-strain curve obtained from compression testing of solid cylindrical sample is used for finite element simulation of four different lattice configurations. The ultimate compressive stress value assigned is 743.3 Mpa at a plastic strain of 0.36 which is obtained from the experimental stress-strain curve. The lower surface of the lattice designs is fixed and the displacement rate is applied on opposite surface to imitate the experimental setup. The simulation is carried for all the designs with same material model, same boundary conditions and the results are presented in following sections.

Table 3.3-1: Material properties used for finite element analysis

| **Properties** | **Value** |
|---|---|
| **Young's Modulus** | 2508.4 Mpa |
| **Poisson's ratio** | 0.3 |
| **Ultimate Compressive Strength** | 743.3 Mpa |

### 3.3.1 Finite element simulation of solid

The experimental strain-stress curve was obtained from load-displacement data and compared to that of curve obtained using FE simulation. Figure 3.3-1a shows the comparison between stress-strain curves and Figure 3.3-1b shows the deformed sample under simulated compression load. Comparison between experimental and simulation results shows the capability of material model to reproduce stress-strain curve with very good accuracy as shown in Figure 3.3-1a. Therefore, material properties obtained from experimental testing of binder jet made stainless steel solid is capable of accurately simulating the compressive behavior using ANSYS. Figure 3.3-2 shows change in sample cross section at various stages in experimental compression testing.

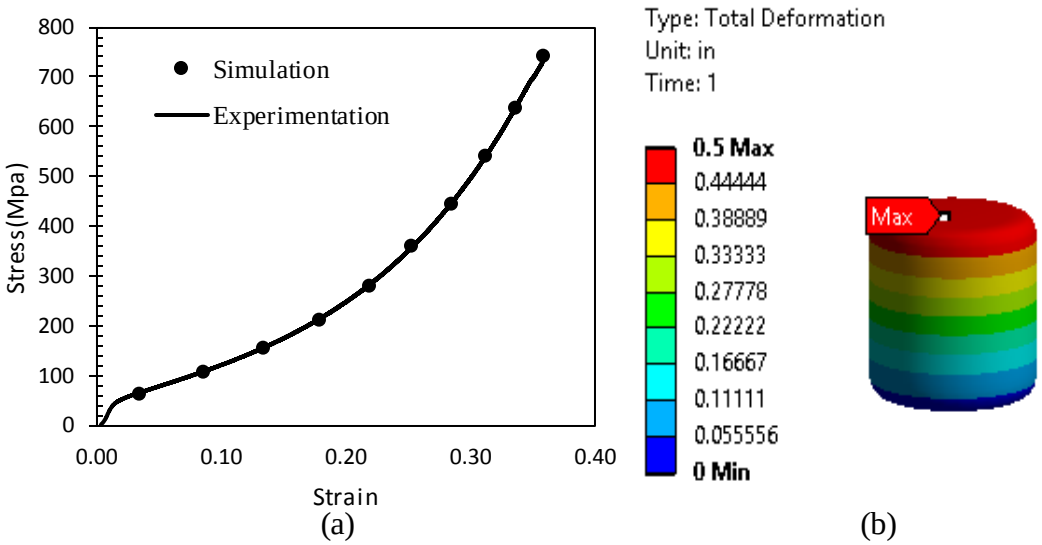


Figure 3.3-1: (a) Comparison between experimental and simulation results of compression test (b) Deformation of solid analyzed in FE simulation

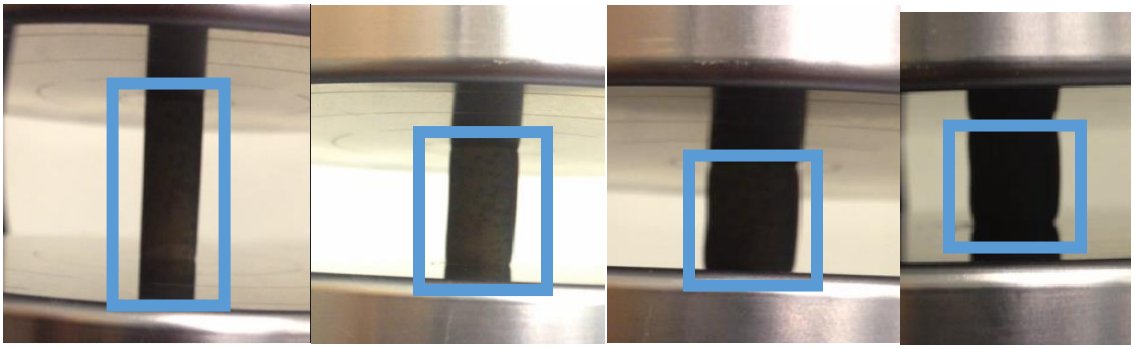

Figure 3.3-2: Change in sample cross section during compression testing

### 3.3.2 Finite element simulation of four lattice structures

The same plasticity material model was used for all the designs and the compressive behavior was simulated. As it is nonlinear analysis, high mesh density is required to capture accurate results. The load-displacement results from simulation were compared to that of experimental test load-displacement results and are shown in Figure 3.3-3 and stress-strain curve comparison doesn't give better comparative results as the stress and strain measured from experiments is not at critical locations.

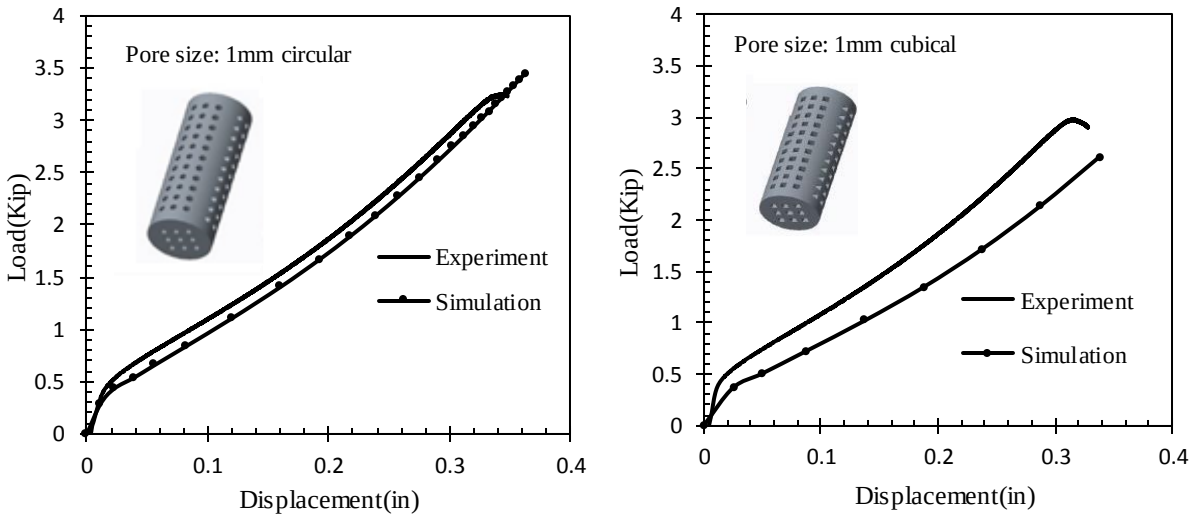


(a) (b)

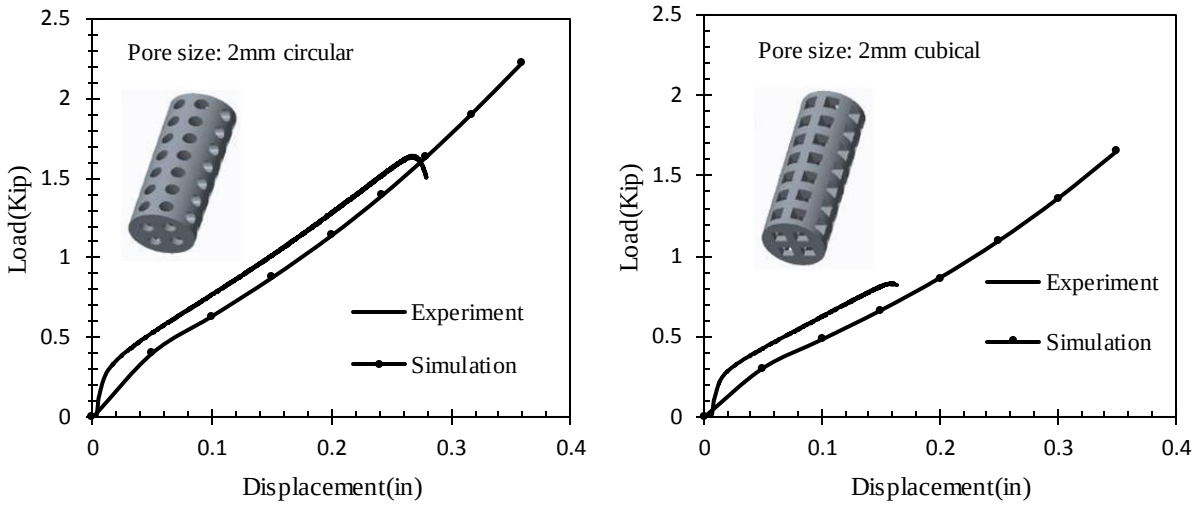


Figure 3.3-3: Load-Displacement curve comparison of simulation with experimental data. (a) Circular1, (b) Cubical 1, (c) Circular 2, (d) Cubical 2

Deformed images of samples during FE simulation and experimental testing is shown in Figure 3.3-4 and Figure 3.3-5 respectively. The displacements induced in experimentation and Finite element simulation are similar and all the lattice structures shown the maximum displacement at the surface where load applied and the lowest at supporting surface.

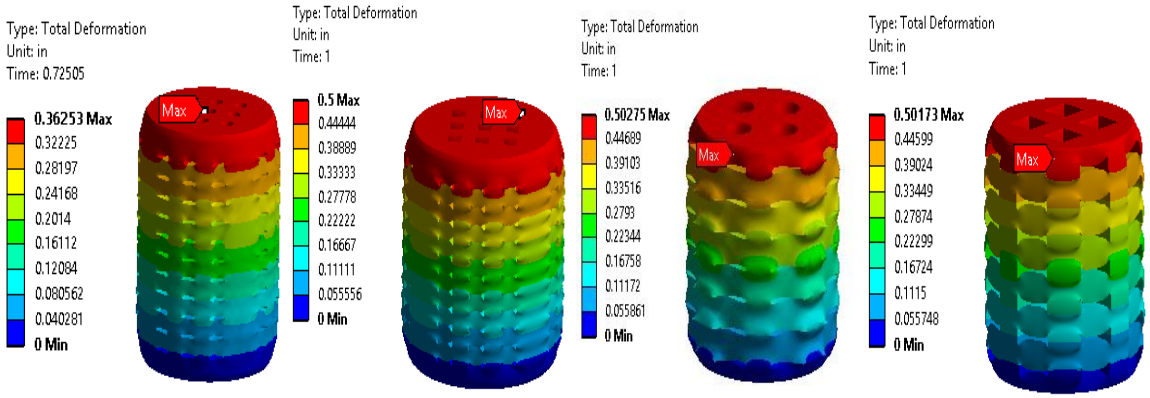


(a) (b) (c) (d)

Figure 3.3-4: Deformed images of FE simulation (a) Circular 1, (b) Cubical 1, (c) Circular 2 and (d) Cubical 2

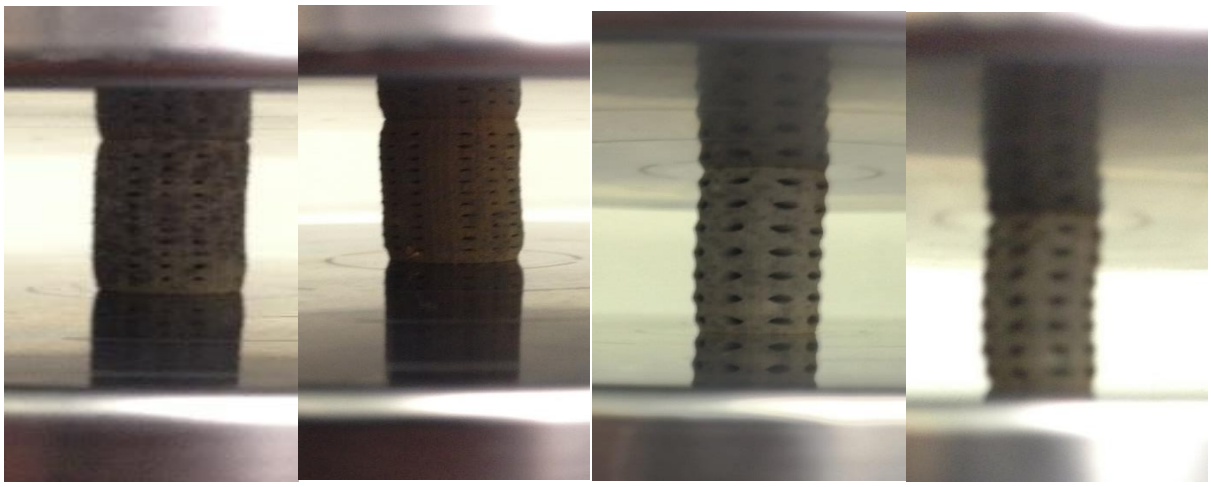

(a) (b) (c) (d)

Figure 3.3-5: Deformed images during compression testing (a) Circular 1, (b) Cubical 1, (c) Circular 2 and (d) Cubical 2.

The ultimate compressive load and stiffness obtained using FE simulation and experimental tests, the difference between actual and FE compressive strengths are represented in Table 3.3-2. The percentage difference in ultimate compressive loads of cubical1, circular1 are less compared to that cubical2 and circular2 structures.

Table 3.3-2: Experimental and FE results

| Name | Numerical Stiffness (lbs/in) | Experimental Stiffness (lbs/in) | Numerical Compressive Load(Kips) | Experimental Compressive Load(Kips) | Difference (%) |
|---|---|---|---|---|---|
| **Cubical1** | 7000 | 7700 | 2.6148 | 2.969 | 13.5 |
| **Circular1** | 7800 | 7500 | 3.4523 | 3.268 | 5.3 |
| **Cubical2** | 3600 | 3800 | 1.6507 | 0.8321 | 49.5 |
| **Circular2** | 5090 | 5400 | 2.224 | 1.6355 | 26.4 |

The comparison of ultimate compressive load obtained from simulation and compression testing shows the difference of 5.3 % for circular1, 13.5% for cubical, 26.4% for circular2, 49.5% for cubical2 lattices. It can be concluded that difference is less for less porous structures like 1000µm pore sized structures compared to 2000µm pore sized structures, the difference in prediction increases with increase in porosity of samples. In order to achieve the accurate results, more

mechanical tests along with thermal examination has to be performed on solid cylinder to make the material model account for the real material behavior. The nonlinear analysis involving plastic deformation needs high mesh density to capture the results more accurately and also the reason of error could be from the fact that the finite element solvers doesn't account for porosity, the sample is assumed to be made from conventional manufacturing or subtractive manufacturing and also the solver assumes there is no force in directions other than the one in which loading takes place. The material model is still preliminary model, it can be improved and the difference would have been less if the material accounts for overall failure.

## 3.4 APPLICATIONS

Binder jet additive manufacturing is still in its preliminary research stage compared to other metal additive manufacturing technologies like selective laser melting, direct metal laser sintering, especially in order to transit the binder jet additive manufacturing from prototyping to real production lot of research has to be established. The current study of process-parameter optimization serves as guideline to adjust the printing parameters for fabrication of variety of materials for different applications and it also helps to better understand the machine for fabricating quality products. Process-property optimization study suggests the set of process parameters to achieve desired compressive strength with low shrinkage rates, reducing the experimentation cost.

The entire binder jetting process is shown in Figure 3.4-1. It can be seen there are lot of phenomena which effects the overall characteristics of final product.

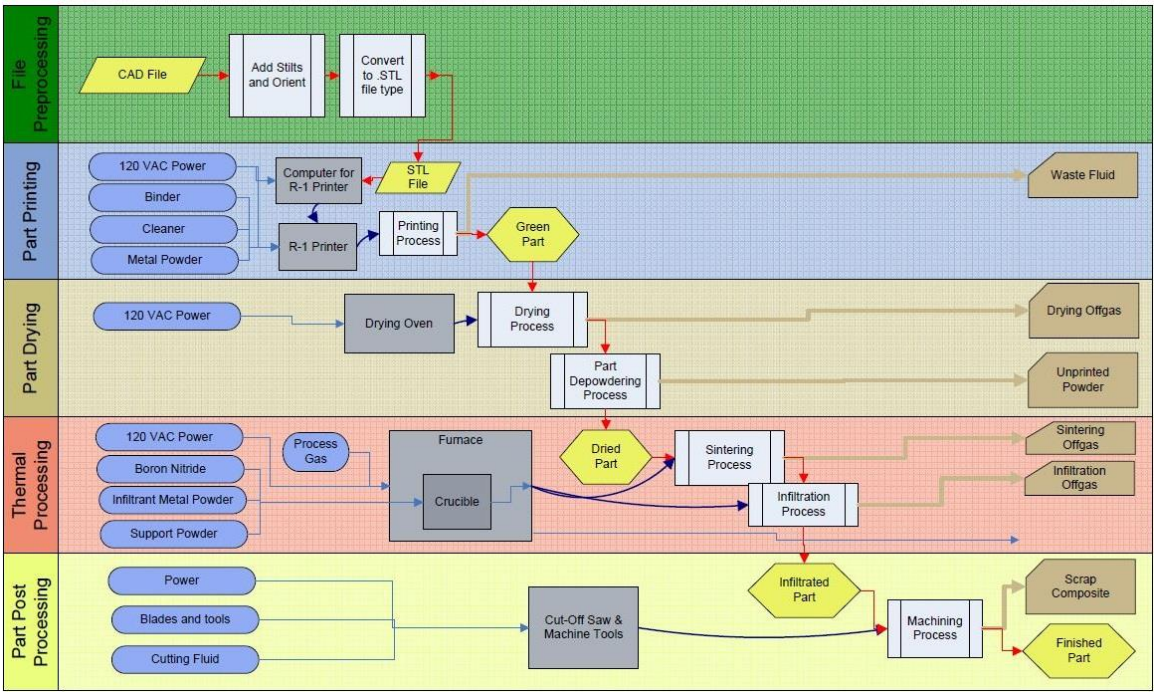


Figure 3.4-1: Flowchart representing the complete binder jetting process [66]

Physical modelling of binder jet additive manufacturing is almost impossible as it involves lot of phenomena like CAD to STL conversion, binder powder reaction, heat treatment, information exchange, powder chemistry. There has to be data-driven model which serves as a guide to quantify the relationship between input and output parameters. The current neural network model helps to identify the set of parameters to achieve desired compressive strength eliminating the need of experimentation.

It is also important to have finite element models of binder jet made samples so that the technology can be deployed for specific application, one such important application is bone scaffold engineering. Finite element models are useful for stress-strain analysis, determination of mechanical properties and helps in design optimization of scaffolds/implants. The current FE study serves as starting point for more research on finite element modelling of binder jet made samples using experimentation.

## 3.5 CONCLUSION AND SUGGESTION FOR FUTURE WORK

Stainless steel cylindrical samples were fabricated for each run of experimental plan with different process parameters. Layer thickness, sintering time and sintering temperature were analyzed to the study its effect on compressive strength and shrinkage rates. The optimized response considered in the study are high compressive strength, low radial and longitudinal shrinkage rates. Visualization plots shows that layer thickness has most influence on compressive strength whereas sintering time has higher influence on radial and longitudinal shrinkage rates. The optimal parameters for high compressive strength are 50µm layer thickness, 4 hours sintering time and 1180 $^{o}$C sintering temperature and for low shrinkage rates are 100µm layer thickness, 2 hours sintering time and 1120 $^{o}$C sintering temperature. The identified optimal parameters might not be same for different material, but the study serves as guidelines to adjust printing parameters for different materials. Along with parameter optimization, the study also investigated the application of artificial neural network for property prediction and a numerical model was developed using feed forward back propagation neural network shows the predictive capability of 2.75%, 4.15% and 9.16% for three different test cases and the predictive capability gets better with repeated training and the model validation was done with data from the literature. The developed model predicts the compressive strength given the input parameters and it serves as framework to set the process parameters to achieve desired output characteristics, thus saving experimental costs.

Finite element models of different designs were developed using the material data obtained from compression testing of solid cylinder, the compressive behavior of different designs was simulated using Finite element software package ANSYS. The comparison of load-displacement curves obtained from simulation and compression testing shows accurate results for solid and are in good agreement for 1000 µm pore sized lattice structure with difference being less than 13.5%,

compared to that of 2000 µm pore sized lattice structures. The material model needs to be made accountable by conducting several mechanical tests like tensile test, volumetric compression test, and shear test. The study serves as starting point for simulating the binder jetting made sample using experimental data.

In the current study, only three important parameters were considered to study their effect on mechanical properties. Furthermore, three more process parameters like powder characteristics, binder saturation, printing orientation can be considered for the studying their effect on output characteristics. Also, the same work can be extended for other materials for different applications using binder jet additive manufacturing.

As more parameters are explored, more input and output parameters can be included in the neural model making the model prediction become accurate. More experiments should be conducted to collect more data, training the network with more data improves the prediction accuracy. Also, more mechanical tests as to be performed to make the finite element material model accountable for overall mechanical behavior.

Once the material model is established, it will be of interest to carry out structure optimization of binder jet made samples. In the current study with lattice structures of two shapes and unit cells, shape and topology optimization studies would be of greater interest as the optimization of lattice structures using additive manufacturing has numerous applications in aerospace, automotive and biomedical industries.

# 4 BIBLIOGRAPHY


[1] A. Butscher, M. Bohner, S. Hofmann, S. Gauckler and R. Müller, "Structural and material approaches to bone tissue engineering in powder-based three-dimensional printing," *ActaBiomaterialia,* p. 907–920, 2011.

[2] A. Butscher, M. Bohner, C. Roth, A. Ernstberger and R. Heuberger, "Printability of calcium phosphate powders for three-dimensional printing of tissue engineering scaffolds," *ActaBiomaterialia,* pp. 373-385, 2012.

[3] S. Bose, S. Vahabzadeh and A. Bandyopadhyay, "Bone tissue engineering using 3D printing," *Materialstoday,* vol. 16, no. 12, pp. 496-504, 2013.

[4] M. Barak and A. Black, "Using 3D-Printing to Evaluate Trabecular Bone Mechanical Properties," *The FASEB Journal,* vol. 31.

[5] "Standard terminology for additive manufacturing technologies," *ASTM-F2792-12a,* 2013.

[6] O. Mohamed, S. Masood and J. Bhowmik, "Optimization of Fused Deposition Modeling Process Parameters:A Review of Current Research and Future Prospects," *Advanced Manufacturing,* vol. 3, pp. 42-53, 2015.

[7] P. Patel, J. Patel and K. Maniya, "Evaluation of FDM Process Parameter for PLA Material by Using MOORA-TOPSIS Metho," *International Journal of Mechanical and Industrial Technology,* vol. 3, no. 1, pp. 84-93, 2015.

[8] G. Onwubolu and F. Rayegani, "Characterization and Optimization of Mechanical Properties of ABS Parts Manufactured by the Fused Deposition Modeling Process," *International Journal of Manufacturing Engineering Volume,* 2014.

[9] K. Christiyana, U. Chandrasekhar and K. Venkateswarlu, "A study on the influence of process parameters on the Mechanical Properties of 3D printed ABS composite," *Material Science Engineering.*

[10] K. Bakshi and A. Mulay, "A Review on Selective Laser Sintering: A Rapid Prototyping Technology," *IOSR Journal of Mechanical & Civil Engineering (IOSRJMCE),* pp. 53-57.

[11] W. Ruban, V. VijayaKumar, P. Dhanabal and T. Pridhar, "Effective Process Parameters in Selective laser sintering," *International journal of Rapid Manufacturing,* vol. 4, no. 2-4.

[12] Z. Liu, J. Nolte, J. Packard, G. Hilmas, F. Dogan and M. Leu, "Selective Laser Sintering of High density Alumina Ceramic Parts," in *35th International MATADOR Conference*.

[13] J. Liu, B. Zhang, C. Yan and Y. Shi, "The effect of processing parameters on characteristics of selective laser sintering dental glass-ceramic powder," *Rapid Prototyping Journal,* vol. 16, no. 2, pp. 138-145, 2010.

[14] A. Wegner and G. Witt, "Correlation of process parameters and part properties in laser sintering using response surface modelling," *Physics Procedia ,* vol. 39, pp. 480-490, 2012.

[15] E. Hofland, I. Baran and D. Wismeijer, "Correlation of Process Parameters with Mechanical Properties of Laser Sintered PA12 Parts," *Advances in Materials Science and Engineering Volume ,* 2017.

[16] A. Kampker, K. Kreisköther and C. Reinders, "Material and Parameter Analysis of the PolyJet Process for Mold Making Using Design of Experiments," *International Journal of Chemical, Molecular, Nuclear, Materials and Metallurgical Engineering,* vol. 11, no. 3.

[17] A. Kesy and J. Kotlinski, "Mechanical properties of parts produced by using polymer jetting technology," *Archives of Civil and Mechanical Engineering,* vol. 10, no. 3, 2010.

[18] K. Wong and A. Hernandez, "A Review of Additive Manufacturing," *ISRN Mechanical Engineering,* 2012.

[19] Gibson, D. Rosen and B. Stucker, Additive manufacturing technologies, Springer, 2010.

[20] A. Jansson and O. Edholm, "Scale factor and shrinkage in additive manufacturing using binder jetting," in *Stockhol,* Sverige, 2016.

[21] J. Gonzalez, J. Mireles, Y. Lin and R. Wicker, "Characterization of ceramic components fabricated using binder jetting additive manufacturing technology," *Ceramics International,* vol. 42, no. 9.

[22] A. Yao and Y. Tseng, "A robust process optimization for a powder type rapid prototyper," *Rapid Prototyping Journal,* vol. 8, pp. 180-189, 2002.

[23] V. Mohammad and C. Chua, "Effects of layer thickness and binder saturation level parameters on 3D printing process," *International Journal of Advanced Manufacturing Technology,* vol. 53, no. 1-4, pp. 275-284, 2010.

[24] T. Hsu and W. Lai, "Manufacturing parts optimization in the three-dimensional printing process by the Taguchi method," *Journal of Chinese institute of Engineers,* pp. 121-130, 2010.

[25] S. Shrestha and G. Manogharan, "Optimization of Binder Jetting Using Taguchi Method," *JOM Additive Manufacturing,* vol. 69, no. 3, pp. 491-497, 2017.

[26] J. Suwanprateeb, F. Thammarakcharoen, K. Wasoontararat and W. Suvannapruk, "Influence of printing parameters on the transformation efficiency of 3D-printed plaster of paris to hydroxyapatite and its properties," *Rapid Prototyping Journal,* vol. 18, p. 4, 2012.

[27] C. Han and F. Yaoyao, "Process parameters optimization for improving surface quality and manufacturing accuracy of binder jetting additive manufacturing process," *Rapid Prototyping Journal,* vol. 22, no. 3, pp. 527-538, 2016.

[28] Y. Tang, Y. Zhou, T. Hoff, M. Garon and Y. Zhao, "Elastic modulus of 316 stainless steel lattice structure fabricated via binder jetting process," *Material Science Technology,* vol. 32, p. 648, 2016.

[29] Y. Bai and C. Williams, "An exploration of binder jetting of copper," Design, Research, and Education for Additive Manufacturing Systems Laboratory.

[30] M. Doyle, K. Agarwal, K. Sealy and K. Schull, "Effect of layer thickness and orientation on mechanical behavior of binder jet stainless steel 420+ bronze parts," *Procedia Manufacturing,* vol. 1, pp. 251-262, 2015.

[31] A. Ihom and A. Offiong, "Neural Networks in Material science and Engineering: A review of sailent isssues," *European journal of engineering and technology,* vol. 3, 2015.

[32] O. Awodele and O. Jegede, "Neural Networks and Its Application in Engineering," in *Informing Science & IT Education Conference* , 2009.

[33] T. Cundari and E. Moody, "A comparison of neural networks versus quantum mechanics for inorganic systems," *Journal of Chemical Information and Computer Sciences,* vol. 37, no. 5, pp. 871-875, 1997.

[34] Y. Asada, E. Nakada, S. Matsumoto and H. Uesaka, "Prediction of t-c for yba2cu3oz doped with ca using neural network," *Journal of Superconductivity,* vol. 10, no. 1, pp. 23-26, 1997.

[35] W. Vermeulen, P. Morris, A. deWeijer and S. VanderZwaag, "Prediction of martensite start temperature using artificial neural networks," *Ironmaking Steelmaking,* vol. 23, no. 5, pp. 433-437, 1996.

[36] Y. Al-Assaf and H. Kadi, "Fatigue life prediction of unidirectional glass fiber/epoxy composite laminae using neural networks," *Composite Structures,* vol. 53, no. 1, pp. 65-71, 2001.

[37] D. Scott, P. Coveney, J. Kilner, J. Rossiny and N. Alford, "Prediction of the functional properties of ceramic materials from composition using artificial neural networks," *Journal of the European Ceramic Society,* 2007.

[38] B. Zahran, "Using neural networks to predict the hardness of aluminum alloys," *Engineering, Technology & Applied Science Research,* vol. 5, no. 1, pp. 757-759, 2015.

[39] M. Eydivanda, M. Hashjinb, A. Fathic, M. Padashic and N. Osmana, "Optimal Design of a 3D-printed Scaffold Using Intelligent Evolutionary Algorithms," *Applied Soft Computing,* vol. 39, pp. 36-47, 2016.

[40] G. Tourloukis, S. Stoyanov and T. Tilford, "Predictive modelling for 3D inkjet printing processes," in *Electronics Technology(ISSE),* 2016.

[41] N. H, "Fabrication, properties and application of porous metals with directional pores," *Progress in Material Science,* vol. 52, 2007.

[42] A. Evans, J. Hutchinson, N. Fleck, M. Ashby and H. Wadley, "The topological design of multifunctional cellular metals," *Progress in Material Science,* vol. 46, 2001.

[43] O. Harrysson, O. Cansizoglu, C. D, H. West and T. Mahale, "Properties of Ti–6Al–4V non-stochastic lattice structures fabricated via electron beam melting," *Material Science Engineering,* 2008.

[44] H. Wadley, "Cellular metals manufacturing," *Advance Engineering Materials,* vol. 4, pp. 726-733, 2002.

[45] O. Iyibilgin, C. Yigit and M. Leu, " Experimental investigation of different cellular lattice structures manufactured by fused deposition modeling," in *Solid freeform fabrication,* 2013.

[46] L. Mullen, R. Stamp, W. Brooks, E. Jones and C. Sutcliffe, "Selective laser melting: a regular unit cell approach for the manufacture of porous, titanium, bone in-growth constructs, suitable for orthopedic applications," *Journal of Biomedical Research,* vol. 89, 2009.

[47] C. Yan, L. Hao, A. Hussein, P. Young and D. Raymont, "Advanced lightweight 316L stainless steel cellular lattice structures fabricated via selective laser melting," *Materials and Design,* 2013.

[48] N. Contuzzi, S. Campanelli, C. Casavola and L. Lamberti, "Manufacturing and Characterization of 18Ni Marage 300 Lattice Components by Selective Laser Melting," *Materials,* vol. 6, pp. 3451-3468, 2013.

[49] S. M. Ahmadi, S. Yavari, R. Wauthle, B. Pouran, J. Schrooten, H. Weinans and A. Zadpoor, "Additively Manufactured Open-Cell Porous Biomaterials Made from Six Different Space-Filling Unit Cells: The Mechanical and Morphological Properties," *Materials,* vol. 8, pp. 1871-1896, 2015.

[50] A. Farzadi, M. Hashjin, M. Eydivand and N. Osman, "Effect of Layer Thickness and Printing Orientation on Mechanical Properties and Dimensional Accuracy of 3D Printed Porous Samples for Bone Tissue Engineering," *PLOS ONE*, 2014.

[51] R. Gorguluarslan, U. Gandhi, R. Mandapati and K. Choi, "Design and fabrication of periodic lattice-based cellular structures," *Computer-Aided Design and Applications,* vol. 13, no. 1, 2016.

[52] C. Beyer and D. Igueroa, "Design and Analysis of Lattice Structures for Additive Manufacturing," *Journal of Manufacturing Science and Technology,* vol. 12, 2016.

[53] H. Brodin and J. Saarimäki, "Mechanical properties of lattice truss structures made of a selective laser melted superalloy," in *13th International Conference on Fracture*, Beijing, 2013.

[54] J. Niu, H. Choo and W. Sun, "Finite element analysis and experimental study of plastic lattice structures manufactured by selective laser sintering," *Journal of Materials: Design and Applications.*

[55] M. Helou, S. Vongbunyong and S. Kara, "Finite Element Analysis and Validation of Cellular Structures," *ScienceDirect, Procedia* , pp. 94-99, 2016.

[56] U. Ajoku, N. Hopkinson and M. Caine, "Experimental measurement and finite element modeling of the compressive properties of laser sintered Nylon-12," *Materials Science and Engineering,* pp. 211-216, 2006.

[57] C. Neff, N. Hopkinson and N. Crane, "Selective Laser Sintering of Diamond Lattice Structures: Experimental Results and FEA Model Comparison," University of South Florida, Tampa.

[58] K. Kolan, M. Leu, G. Hilmas and T. Comte, "Effect of Architecture and Porosity on Mechanical Properties of Borate Glass Scaffolds Made by Selective Laser Sintering," in *SFF Syposium*, 2013.

[59] B. Langranda, F. Casadeib, V. Marcadona, G. Portemonta and S. Krucha, "FE modeling of cellular materials under compressive load," *Procedia Engineering,* p. 1951 – 1958, 2017.

[60] "Standard Test Methods of Compression Testing of Metallic Materials at Room Temperature".*ASTM International, Designation: E9-09.*

[61] K. Kolan, M. Leu, G. Hilmas, R. Brown and M. Velez, "Fabrication of 13-93 bioactive glass scaffolds for bone tissue engineering using indirect selective laser sintering," *Biofabrication,* vol. 3, 2011.

[62] R. German, Sintering Theory and Practice, John Wiley & Sons Inc, 1996.

[63] J. Sola and J. Sevilla, "Importance of input data normalization for the application of neural networks to complex industrial problems," *IEEE Transactions on Nuclear Science,* vol. 44, no. 3, 1997.

[64] T. Nguyen, Y. Yang, K. Bae and S. Choi, "Prediction of deformation of steel plate by artificial neural network in forming process with induction heating," *Journal of Mechanical Science and Technology,* vol. 23, 2009.

[65] R. Singh, R. Gupta and S. Sarkar, "Application of artificial neural network for prediction of hardness of shielded metal arc welded joints under the influence of external magnetic field," *International Journal of Engineering Research and Development*.

[66] C. Ingenthron, "The Effects of Layer Thickness on Dry-Sliding Wear of Binder Jet Additively Manufactured Stainless Steel and Bronze Composite," Cornerstone:Minnesota State University, Mankato, 2015.